論文 / 著書情報
Article / Book Information

題目(和文)	逆層交換型アルミニウム誘起シリコン結晶化プロセスにおける不純物効果の研究
Title(English)	Study on Impurity Effect in Inverted Aluminum-Induced Layer Exchange Process for Polycrystalline Silicon Thin Films
著者(和文)	竹内正芳
Author(English)	Masayoshi Takeuchi
出典(和文)	学位:博士(工学), 学位授与機関:東京工業大学, 報告番号:甲第9490号, 授与年月日:2014年3月26日, 学位の種別:課程博士, 審査員:近藤 道雄,小田原 修,吉本 護,半那 純一,和田 裕之
Citation(English)	Degree:Doctor (Engineering), Conferring organization: Tokyo Institute of Technology, Report number:甲第9490号, Conferred date:2014/3/26, Degree Type:Course doctor, Examiner:Michio Kondo,Osamu Odawara,Mamoru Yoshimoto,Junichi Hanna,Hiroyuki Wada
学位種別(和文)	博士論文
Type(English)	Doctoral Thesis

Doctoral Thesis

Study on Impurity Effect in Inverted Aluminum-Induced Layer Exchange Process for Polycrystalline Silicon Thin Films

Masayoshi Takeuchi

Department on Innovative and Engineered Materials

Interdisciplinary Graduate School of Science and Engineering

Tokyo Institute of Technology

March 2014

Synopsis

Large-grained polycrystalline silicon (poly-Si) thin films on insulating substrates are attractive for the fabrication of thin film silicon solar cells. Although a great number of researches have been performed to realize insulating substrates with large-grained poly-Si thin films at the surface, none of them have achieved high efficiency thin film silicon solar cells.

In this study, an aluminum-induced layer exchange (ALILE) process, with employs a precursor sample with inverted layer sequence in contrast to conventional structure, is studied. The ALILE is named “inverted-ALILE”. Considering that conventional ALILE process leads to layer exchange of amorphous silicon (a-Si) and aluminum and concurrent crystallization of a-Si, inverted-ALILE process is expected to form a final layer structure of glass/Al-rich/poly-Si from the precursor structure of glass/a-Si/Al. After annealing, a poly-Si layer is formed on the top surface and an aluminum-rich metallic layer with small portion of Si is formed between the poly-Si layer and insulating substrate which can act as aback electrode for solar cells. As a result, the obtained solar cell has a highly conductive layer at the bottom, which is more favorable for high efficiency solar cell than the coplanar structure obtained by conventional ALILE process. A metallic layer formed between the poly-Si layer and insulating substrate can also function as a reflecting layer, so that higher current density is expected owing to effective light trapping. In addition, the crystal orientation of the poly-Si layer is studied. Si(100) is essential for texturing antireflection structures and Si(111) is useful as epitaxial templates for advanced solar-cell materials.

In chapter 1 “Introduction”, the background of this study is started.

In chapter 2 “Experiment details”, preparation method of the precursor sample for inverted-ALILE process is described. Annealing apparatus and basic annealing conductions are also shown. Characterization techniques of structural and electrical properties employ employed in this are detailed.

In chapter 3, the thickness-modulated inverted-ALILE crystallization technique enables to control the orientation of polycrystalline Si films on glass substrates. The (111) –orientation fraction reached 94.8% for the 45nm-thick sample. This mechanism was discussed in terms of the heterogeneous nucleation energy.

In Chapter 4, requirements for the realization of inverted-ALILE process, which means the formation of both large-grained poly-Si layer and aluminum-rich bottom layer on glass substrate, are discussed. Influence of impurity in precursor a-Si sample is also demonstrated.

In chapter 5, inverted-ALILE samples are applied to thin film silicon solar cells fabrication. Fabrication procedures of solar cells using these inverted-ALILE samples were evaluated.

In the final chapter, conclusions obtained through this work are summarized.

Contents

Chapter 1

General introduction

1.1 Background

In a world where a rapidly increasing demand for energy is ever more strongly conflicting with an urgent need to cut back on greenhouse gas emissions, it seems necessary and inevitable that renewable energy sources will play a major role in our future global energy system. In 2013, Conference of the parties 19 (COP19) was held in Warsaw and world minister discussed challenges for greenhouse gas emission reduction new target. Japan's previous target was to slash emissions by 25 percent compared to fiscal 1990 levels, which was decided in 2009 by then Prime Minister Yukio Hatoyama. The new target announced for curtailing greenhouse gas emissions by 3.8 percent from fiscal 2005 levels by fiscal 2020. From the worldwide viewpoint, International Energy Association (IEA) has proposed to increase contribution of solar cells to 26% of whole electric generation in the world by 2040. On the other hand, total production of solar cells in the world increases at an annualized rate exponentially. As a result, cumulated production attained to 32.1GW by the year of 2011 as shown in Fig.1.1. [1] Even through production of solar cells will continue increasing, no one knows which kind of solar cells dominates the market in the future.

During the last decade, the production of solar cells has grown dramatically. With a

shape of 86.8%, (Fig.1.2) wafer-based crystalline silicon solar cells are still dominating the market, which are called *first generation solar cells*. In order to maintain high growth rates in the future, significant cost reductions are necessary. The reduction of the silicon thickness is an appealing way to bring down costs because even relatively thin crystalline Si solar cells feature the potential for high efficiencies. The potential has already been demonstrated by the preparation of a solar cell with an efficiency of 21.5% on a thinned-down monocrystalline Si wafer with a thickness of 47μm [2]. Unfortunately, this is not a real Si thin-film technology but still a Si wafer technology. In order to bring down coats substantially, high efficiencies have to be reached with a real Si thin-film technology utilizing competitive production techniques for large-area low foreign substrates (e.g., glass).

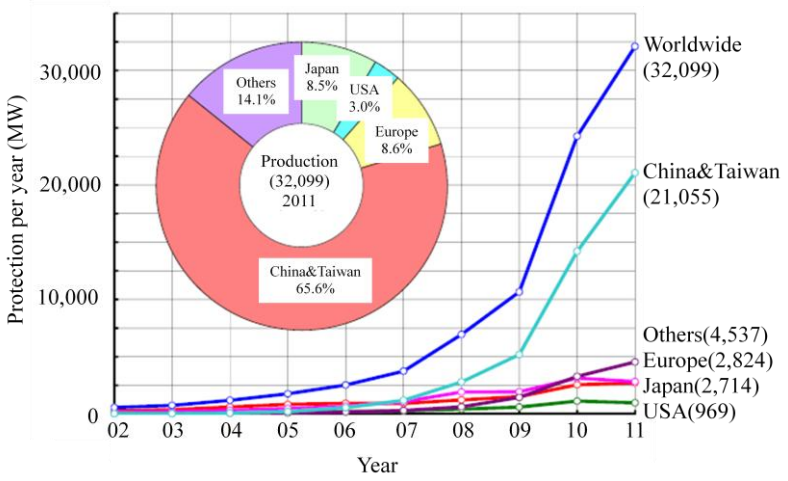

Fig.1.1Production of solar cells in the world[1]

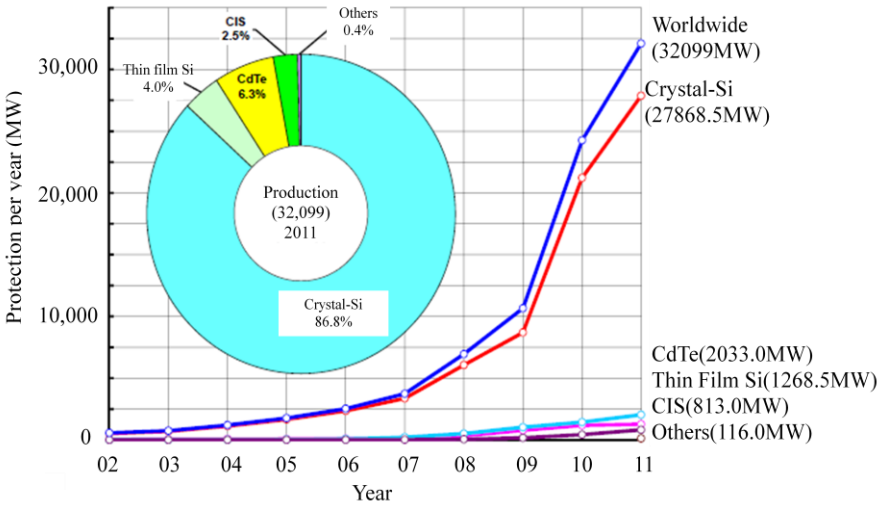

Fig.1.2 Production of solar cells by type[1]

1.2 Thin-film silicon solar cells on foreign substrates

The corresponding process technologies to *second generation solar cells* have been developed together with the microelectronics industry. However, an essential difference between solar cells and other microelectronics lies in scalability. While transistors get cheaper and higher performance as getting smaller, solar cells cannot decrease in size because their energy output is in accordance with the area which absorbs the sunlight. Instead, the efficiency of the device has been increased with various attempts in all solar cell concepts, but is still limited to 30% for an energy gap of 1.1eV [3]. The ideas on how to overcome this theoretical limit was summarized with so called third generation solar cells [4]. The more promising approach on a short to medium term for solar cells is the reduction of material consumption, which will be realized by the reduction of the thickness of solar cells. As described above, thin film concepts are considered *second generation solar cells*. The thickness of the wafer based cells is limited by the mechanical stability during wafer handling. If the mechanical stability issue is

transferred to inexpensive substrates like glass, it can be possible to use much thinner films. Beside PV applications, thin-film technology is also attractive for large area electronic devices such as displays and sensors. Deposition of thin films on large glass substrates has already been developed by using plasma enhanced chemical vapor deposition (PECVD) [5]. The Si thin-film solar cells on glass, available on the market today, are mainly based on hydrogenated amorphous Si (a-Si:H) and hydrogenated microcrystalline Si (μc-Si:H). Both are usually prepared by PECVD. A big advantage of both technologies is that the Si films can be prepared at very low temperatures (below 300^{o}C). Although stabilized single-junction solar cell efficiencies of about 10% have already been reached on small areas in the laboratory (e.g., 10.1% on 1cm^{2} for a-Si:H [6]), both materials probably do not have the potential for very high single junction efficiencies as the structural quality is relatively poor. To reach higher efficiencies, a-Si:H/μc-Si:H tandem solar cells have been developed. An a-Si:H/μc-Si:H tandem cell with initial efficiency of 15.0% was announced as the world record efficiency by the R&D group of Kaneka Corporation[7]

To overcome the current single-junction efficiency limits of both a-Si:H and μc-Si:H, the Si material quality has to be improved substantially. Large grained polycrystalline Si (poly-Si) thin-films, characterized by both (1) a grain size much larger than the film thickness and (2) an intra-grain quality comparable to wafer-based Si, seem to be a suitable material for high efficiency Si thin-film solar cells on glass. The preparation of such large-grained poly-Si films poses a big challenge because the glass substrate limits the process temperatures to about 600^{o}C (the precise temperature limit strongly depends on the type of glass substrate). Due to the fact that the direct deposition of Si on glass

below 600^{o}C always results in amorphous Si and /or fine-crystalline Si (i.e., with a grain size much smaller than the film thickness), the techniques investigated so far are usually based on a two step process. In the first step, an amorphous Si (a-Si) film is deposited and in the second step this a-Si film is crystallized. For example, the a-Si layer can be crystallized thermally at about 600^{o}C (solid phase crystallization: SPC) [8]. At such low temperatures, the process is relatively slow and the Si films formed by SPC feature a grain size comparable to the film thickness (for a film thickness of 1-2μm). Based on SPC, mini-module efficiencies of up to 10.5% have already been obtained [9]. Beside SPC, techniques, such as laser crystallization (LC) [10] and metal-induced crystallization (MIC) [11] have been investigated to form suitable large-grained poly-Si films on glass.

In this chapter, a very specific MIC technique, which is based on aluminum-induced crystallization (AIC) of amorphous Si, is discussed. The associated process is called aluminum-induced layer exchange (ALILE). Here, the resulting poly-Si films are called ALILE films.

1.3Aluminum-induced layer exchange (ALILE)

1.3.1 General aspect of the ALILE process

It is a well known phenomenon that metals can significantly influence the crystallization of amorphous Si. The temperature required to crystallize bare a-Si is about 600^{o}C. The contact of a-Si with metals usually leads to a strong reduction of this crystallization temperature (meal-induced crystallization). For simple eutectic systems

in a layer stack configuration, the MIC process that takes place below the eutectic temperature as a solid phase transition, can be divided into three steps: (1) dissociation of Si atoms from the a-Si into the metal, (2) diffusion of Si atoms through the metal and (3) nucleation and incorporation of Si atoms into already existing Si crystal [12] Due to the fact that Al is shallow acceptor in Si with an energy level of 67mV above the valence band edge, aluminum-induced crystallization of a-Si always leads to p-type material. Over the past decades, AIC has been investigated in different sample structures. In 1977, Majni and Ottaviani investigated a Si-wafer/Al/a-Si structure [13]. The layers (Al and a-Si) were deposited by electron-beam evaporation onto the Si(100) wafer with a thickness of about 700nm each. After annealing at 530 ^{o}C for 12h, an exchange of the two layer positions was observed resulting in a Si-wafer/Si/Al structure. The Si layer had grown epitaxially on the Si(100) wafer and, therefore, the related process is called solid phase epitaxially growth (SPE). Due to doping with Al, the hole concentration of the epitaxially grown p-type Si layer was $2\times10^{18}cm^{-3}$. In 1981, Tsaur *et al*. used this process to form solar cells featuring a p-type SPE-grown Si film to the thickness of about 200nm on a n-type Si wafer[14] . Without antireflection coating (ARC) and back surface filed (BSF), they obtained efficiencies at AM1 of up to 10.4% and 8.5 on mono-crystalline Si(100) wafers and multi-crystalline Si wafers, respectively. In 1998, it was shown that the layer exchange process does not occur on Si wafers only but also on foreign substrates: Koschier et al. demonstrated the process on oxide-covered Si wafer [15] and Nast et al. on glass substrates [16]. Nast *et al*. showed that the utilization of glass substrates leads to the formation of poly-Si films, which are continuous and feature a uniform thickness. In the following years, different aspects of the ALILE process were investigated [17-19].

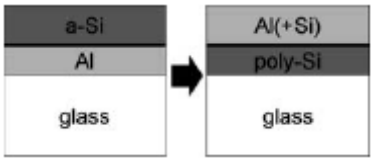

Fig.1.3 Schematic illustration of the aluminum-induced layer exchange (ALILE) process [20]

Starting point for the aluminum-induced layer exchange (ALILE) process on glass is usually a glass/Al/a-Si stack (left hand side of Fig.1.3). Different glass substrates have been used for the process (e.g., Corning 1737, Schott Borofloat 33). The layers (Al and a-Si) are deposited by physical vapor deposition (PVD) (i.e., thermal evaporation, electro-beam evaporation or sputtering). For the deposition of the a-Si layer PECVD has also been used [21] A typical thickness is about 300 and 375nm for the Al layer and the a-Si layer, respectively. The excess of Si compared to Al is necessary for the preparation of continuous poly-Si films on the glass substrate. As already mentioned above, the ALILE process requires a thin permeable membrane (barrier layer) between the Al and the a-Si layer, which controls the diffusion of Al and Si. Usually, the permeable membrane consists of an Al oxide layer formed by exposure to air (e.g., for 2h) of the Al-coated glass substrate prior to the a-Si deposition. Annealing of the initial glass/Al/a-Si stack at temperatures below the eutectic temperature of the Al/Si system (T_{eu}=577^{o}C) leads to a layer exchange and a concurrent crystallization of Si resulting in a glass/poly-Si/Al(+Si) stack (right hand side of Fig. 1.3). The permeable membrane stays in place during the entire ALILE process (indicated by a black line in Fig. 1.3). Thus, the thickness of the resulting poly-Si film is determined by the thickness of the

initial Al layer (in this example about 300nm). Due to the excess of Si, which is necessary to form continuous poly-Si films, the Al layer on the top of the poly-Si film contains some Si inclusion, also referred to as "Si islands."[22]. The amount of Si within the final Al(+Si) layer is determined by the ratio to the thickness of the initial a-Si layer to the thickness of the initial Al layer.

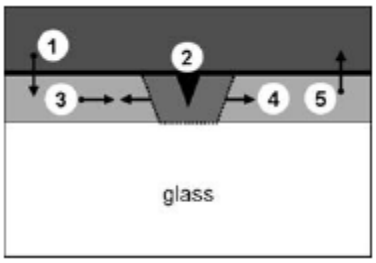

Fig.1.4 Main steps of the aluminum-induced layer exchange (ALILE) process (a glass/Al/a-Si stack is shown) [20]

The main process steps of the layer exchange are schematically depicted in Fig. 1.4 (a glass/Al/a-Si stack is shown with the initial Al layer marked in light gray, the initial a-Si layer in dark gray and the permeable membrane in black). The process starts with the dissociation of a-Si and subsequent diffusion of Si atoms across the permeable membrane into the initial Al layer (process step 1). This leads to an increase in the Si concentration C_{si} within the initial Al layer, until the critical concentration for nucleation is reached. Then, Si nuclei are formed locally within the initial Al layer (process step 2). These nuclei grow in all directions, until they are confined vertically between the glass substrate and the permeable membrane. The Si growth is fed by lateral diffusion of Si atoms within the initial Al layer towards existing grains (process step 3). The Si growth continues only laterally (process step 4), until adjacent grains coalesce and finally, form

a continuous poly-Si film on the glass substrate. Due to the growth of Si grains within the initial Al layer, the Al is displaced to the initial a-Si layer (process step 5) resulting finally in an Al(+Si) layer on top of the poly-Si layer. However, the Al is not completely displaced from the initial Al layer. Some local Al inclusions remain along the grain boundaries of the final poly-Si film.

After the annealing step, the Al was etched off chemically. If the Al is etched off selectively (like in Fig.1.5), the "Si islands" are still on top of the continuous poly-Si film. These islands have the thickness of the original Al layer and vary in size depending on the Si supply. After annealing and Al etching, Si islands were visible in SEM studies. Residual Si, which was dissolved in the Al layer, formed little Si crystals on top of these islands.

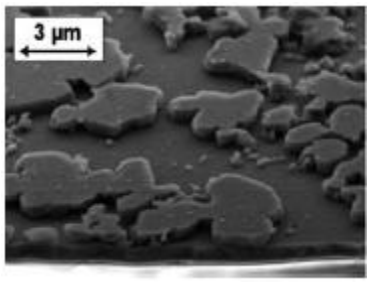

Fig.1.5 SEM image of a poly-Si surface after selective removal of Al by wet chemical etching. In the image the remaining "Si island" are cleary visible. (from [23])

1.3.2 Preferential (100) orientation of the ALILE process

The surface of the poly-Si film is preferentially (100) orientated. This can be seen by the agglomeration of EBSD measurement points close to the (100) corner of the inverse pole figure. To quantify this behavior, the percentage of the measurable area under

investigation, which is titled by less than 20^{o} with respect to the perfect (100) orientation is called the preferential (100) orientation $R_{(100)}$. The corresponding region of the inverse pole figure is indicated by a dashed line (see Fig.1.6 (right)). This definition can also be applied to the (110) and the (111) orientation. The poly-Si film shown in Fig.1.6 features a preferential orientation of 66%, 4%, and 10% for $R_{(100)}$, $R_{(110)}$, and $R_{(111)}$, respectively. This shows clearly the strong preferential (100) orientation of the poly-Si surface [24].

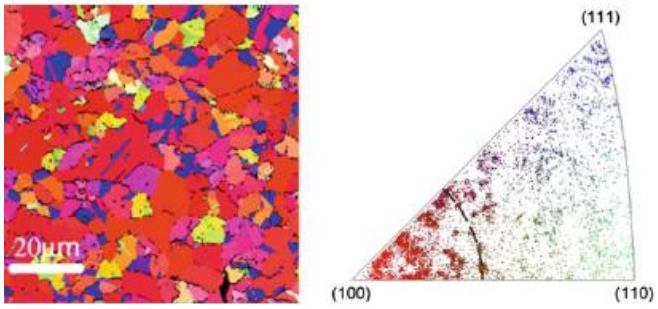

Fig 1.6 Left: Electron backscatter diffraction (EBSD) map showing the grain structure of a poly-Si film on glass prepared by the ALILE process (left) and the corresponding inverse pole figure showing the preferential (100) orientation of poly-Si surface (right). The region used for the definition of the preferential (100) orientation $R_{(100)}$ is indicated by *a dashed line* (20^{o} tilt with respect to the perfect (100) orientation).[24]

1.3.3 Model of the ALILE process

In this section, a model of the ALILE process is described. The five main process steps

of the ALILE process have already been introduced in Fig. 1.4. The silicon, which is required for the growth of existing Si grains, is supplied by lateral diffusion of Si within the Al layer (process step 3). Such a diffusion-limited growth process is based on the fact that the incorporation of dissolved Si atoms into existing Si grains is fast when compared to the diffusion of Si towards existing grains. The diffusion of Si towards existing grains is driven by a gradient of the Si concentration C_{si}. The C_{si} in the direct vicinity of existing grains is lower than far away from the grains. This means that there are Si depletion regions around existing grains [18].

In the first phase of the ALILE process, no stable nuclei are formed (stage I). The formation of stable nuclei starts at the t_0. Nucleation takes usually place only in a short time period. This short time period is called nucleation phase (stage II). After the nucleation phase, no new stable nuclei are formed but the growth of the existing grains continues until the grains coalesce and finally form a continuous poly-Si film on the glass substrate (stage III). The corresponding self-regulated suppression of nucleation, which allows for the growth of large grains, is a characteristic feature of the ALILE process. Nast et al. suggested that the self-regulated suppression of nucleation is due to overlapping Si depletion regions around existing grains [18]. The experimentally observed results regarding nucleation and growth are discussed with the help of the phase diagram of the Al/Si system [25]. The Al-rich part of the phase diagram is shown in the left part of Fig.1.5. In the phase diagram the temperature T is shown versus the C_{si}. The equilibrium lines are indicated as solid lines. At the eutectic temperature of the Al/Si system (T_{eu}=577^{o}C=850K), a maximum of about 1.5at.% Si can be dissolved in solid Al. The ALILE process takes place below the eutectic temperature (e.g., at 750K). This means that the transition occurs directly from the Al phase to the (Al)+(Si) phase.

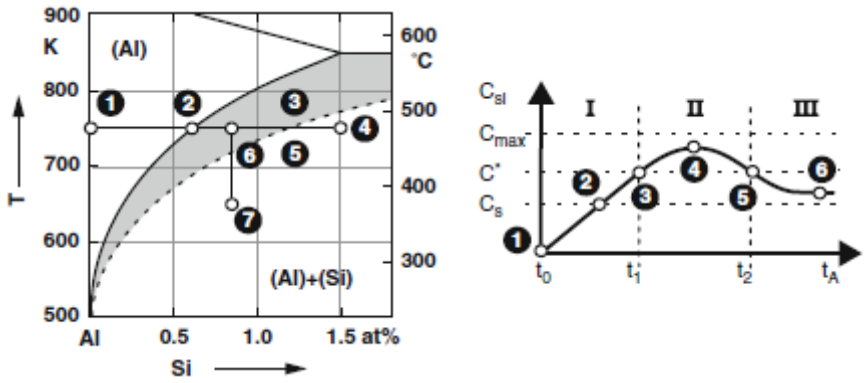

Fig 1.5 Left: Al-rich part of the Al/Si phase diagram. Right: Si concentration C_{si} within the Al layer versus annealing time t_A (C_s: saturation concentration; C^*:critical concentration; C_{max}: maximum concentration) [20]

A key feature of ALILE process is the suppression of nucleation by existing grains and the resulting large grain size of about 10μm. Silicon diffusion towards growing grains leads to the formation of concentration gradients. Fig.1.6 shows in a schematic diagram the silicon concentration profiles between two neighboring grains [18]. The silicon concentration within the grains is indicated by C_g. The growing silicon grain decreases the silicon concentration just in front of the grain to C_i, which is referred to as depletion regions. The silicon concentration is C_n at area far away from the grain, where nucleation is likely to occur. The width of the depletion regions is d. While new nucleation is possible in the supersaturated region between the depletion regions, it is suppressed once the depletion regions overlap. At a distance of $2d$, no further nucleation is possible to occur.

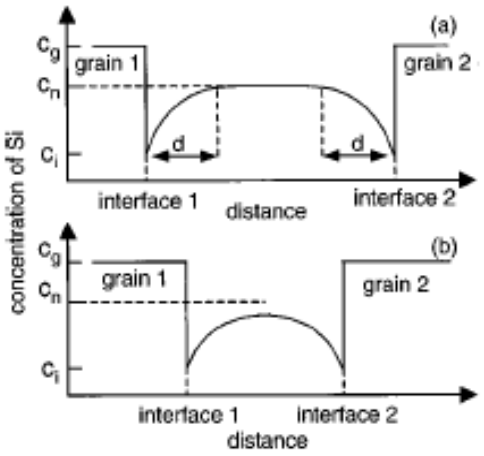

Fig.1.6 A schematic diagram of the silicon concentration profiles between two neighboring grains.[18]

1.3.4 Kinetic model of Si transport into the Al layer

Sarikov et al. shows the orientation of the grains of resulting poly-Si films was investigated using electron back scattering diffraction (EBSD).[26] The respective experimental results for both native and thermal AlOx membranes are shown in Fig. 1.7. The value of $R_{(100)}$ strongly depends on the annealing temperature and the way the membrane was formed. Reducing annealing temperature from 550 down to 450 °C the value of $R_{(100)}$ increased from about 40 to about 70% in the case of native AlOx membrane and from about 10 to about 30% in the case of thermal membrane, respectively. Such influence of the experimental conditions on $R_{(100)}$ finds explanation in the framework of the model of preferential orientation of Si films made by the ALILE process presented in this section.

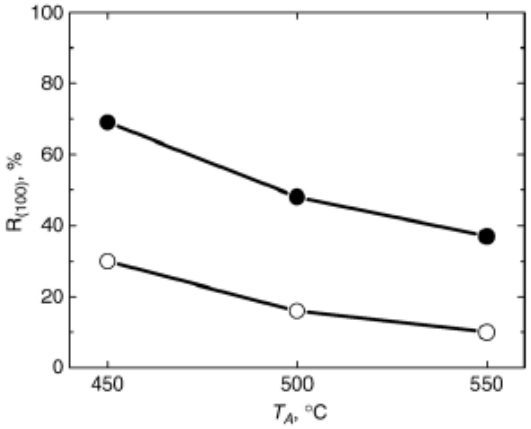

Fig.1.7 Preferential (100) orientation, $R_{(100)}$, as a function of the annealing temperature, T_A, for samples with native oxide (full circles) and thermal oxide (open circles)

The initial layer stack of the ALILE process is initially in a non-equilibrium state. The a-Si and Al layers mutually interact due to the tendency of the overall system to reduce its Gibbs energy. The difference in Gibbs energy between the a-Si and the Al leads to the dissolution of Si, its diffusion in the membrane, and incorporation of the Si into the Al layer (Fig. 1.8). Such a process would in principle continue until the concentration of Si atoms in Al reaches the solubility limit for the amorphous silicon. By this, the local thermodynamic equilibrium at both interfaces a-Si/membrane and membrane/Al and a constant Gibbs energy of Si in the Al layer (and, hence, a constant Si concentration) are assumed.

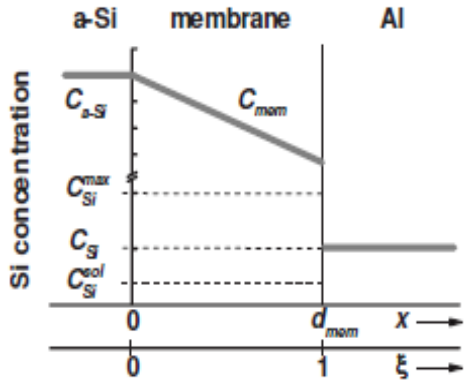

Fig.1.8 Distribution of Si concentration in the a-Si/AlO_x membrane/Al layer stack during the ALILE process. In the figure, $C_{a\text{-}Si}$ is the atomic concentration in amorphous Si, C_{mem} is the Si concentration in the membrane, C_{si}^{max} is the maximum concentration that can enter Al layer in contact with amorphous Si, C_{si} is the Si concentration in the Al layer, and, C_{si}^{sol} is the solubility limit of Si in Al, respectively.

The transport of Si atoms through the membrane is described by the diffusion equation

$$\frac{\partial C_{mem}}{\partial t} = D_{mem} \frac{\partial C_{mem}}{\partial x^2}$$

The introduction of the η and ξ allows to study the dependence of the probability of nucleus orientation on the ratio of interface energies at the AlOx/c-Si and Al/c-Si interfaces (parameter η) as well as on the annealing temperature and the supersaturation of Al with Si (parameter ξ), respectively.

The dependences of the $R_{(100)}$ on η at different values of ξ are shown in Fig. 1.9. Several regions are clearly seen in the curves, which become more pronounced as ξ increases. The preferential (100) orientation of Si grains is observed at $-0.75 \leq \eta \leq 0$ and $0.8 \leq \eta \leq \sqrt{3}$. The degree of preferential orientation in these regions increases with the increase of ξ, which means the decrease of the annealing temperature and/or the supersaturation of Al with Si. The increase of the $R_{(100)}$ with the decrease of annealing temperature is supported by the experimental data in Fig.1.7

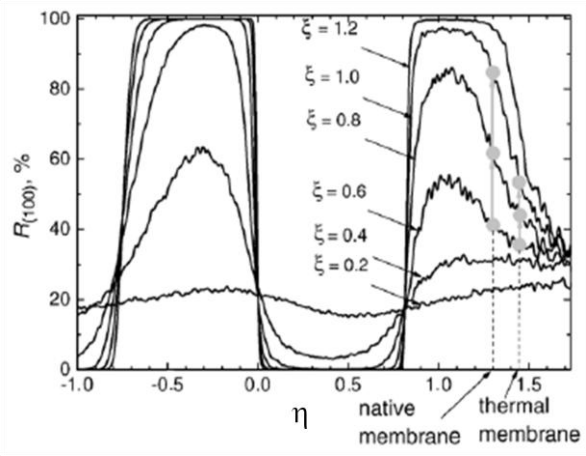

Fig.1.9 Dependences of the calculated R(100) on η at different values of ξ. The behavior of R(100) changing the annealing temperature (the value of ξ) and the technology of the AlO_x membrane (the value of η) is schematically indicated.

A possible solar cell structure using ALILE as seed layers is shown schematically in Fig. 1.7. [27] After depositing the initial aluminum and a-Si layer, the poly-Si layer is formed by ALILE process. An aluminum layer with silicon inclusion is formed on the top of the poly-Si film, which has to be removed. The poly-Si layer is subsequently

thickened by low-temperature epitaxy forming a p-doped absorber. Finally, n^+-emitter is deposited by using a low temperature process such as PECVD. This can either be done epitaxially by changing the dopant or by deposition of an a-SI:H emitter. In the latter case a transparent conducting oxide (TCO) layer is needed to enhance the lateral conductivity of the emitter. A mesa structure has to be fabricated by etching in order to contact the absorber layer. Another deposition of metal contact is also needed in order to prepare electrodes for p-side and grid contact on TCO film.

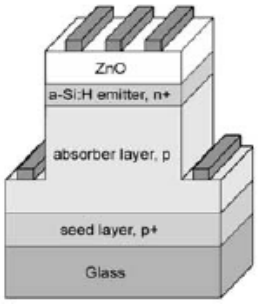

Fig.1.7 A possible solar cell structure using ALILE as a seed layer. [27]

1.3.5 Other Aspects of the ALILE Process

Many groups have studied ALILE process for the sake of realizing high efficiency thin films silicon solar cells. Usually the poly-Si films on foreign substrates, prepared by the ALILE process, are used as a template (seed layer) for subsequent homo-epitaxial growth of the absorber layer of a poly-Si thin-film solar cell. The highest efficiency obtained so far with an ALILE seed layer on foreign substrate is 8% [28]. The corresponding structure of the poly-Si thin-film solar cell is: aluminum substrate/spin-on oxide/p^+-type ALILE seed layer/p^+-type Si BSF (epitaxially

grown)/p-type Si absorber layer (epitaxially growth)/i/n^+-type a-Si:H emitter (grown by PECVD)/indium tin oxide (ITO). The spin-on oxide was used to reduce the roughness of the alumina substrate and, therefore, to increase the grain size of the poly-Si seed layer formed by the ALILE process [29-30]. In this case, the epitaxial thickening of the ALILE seed layer took place at 1130^{o}C using thermal CVD. This high-temperature process is not compatible with the utilization of glass substrates. At temperatures, which are compatible with the utilization of glass substrates (up to about 600^{o}C), the efficiencies obtained so far are much lower. For example, the epitaxial thickening of an ALILE seed layer on glass at about 600^{o}C using high-rate electron-beam evaporation has led to an efficiency of 3.2% [31]. So far, the poly-Si thin-film solar cells on ALILE seed layer are not limited by the grain size but by the intra-grain defects. Therefore, future research will focus on these intra-grain defects.

The poly-Si films obtained by ALILE process always show p-type behavior. On high temperature resistant foreign substrates, the p-type poly-Si can be transferred to n-type poly-Si by overdoping, e.g., by phosphorous diffusion at 950^{o}C [32]. This allows for other solar cell configurations (e.g., substrate/ n^+-type ALILE seed layer/n-type absorber/p^+-type emitter).

For applications, the possibility to form poly-Si films also on conductive foreign substrate is of high importance. It was shown that the ALILE process works also on some metal-coated glass [33]. Especially, the results on ZnO:Al is a well established material for thin-film solar cells. On ZnO:Al-coated glass the grain size of poly-Si film is slightly reduced and its preferential (100) orientation remains about the same (compared to bare glass) [24] It was found that the ZnO:Al does not an degrade during the ALILE process but the conductivity is even improved due to an increased carrier

density [33].

1.4 Inverted-ALILE

The layer exchange not only occurs for the above mentioned layer sequence (“normal structure”), but also for the “inverse structure” [34-35]. In this case, an initial glass/a-Si/Al stack is transformed into a glass/Al-rich/poly-Si stack. The “inverse structure” requires a permeable membrane, too. This membrane can also be prepared by exposure to air. But this time, a Si oxide layer is formed. In comparison with the creation of an Al oxide layer, the Si oxide layer formation takes much longer duration (days instead of hours), because a-Si is not as reactive as Al, regarding oxide formation. It is very remarkable that the layer exchange takes place even if completely different permeable membranes are used. On oxidize wafers, the “inverse structure” was already investigated in 1996 [36].

Kuraseko *et al*. fabricated p-i-n structure with inverted-ALILE sample (Fig.1.7). I-V characteristic of the fabricated solar cell are Jsc of 19.6mA/cm2, Voc of 0.402 V, FF of 0.45 and conversion efficiency of 3.54%[38]. The “inverse structure” has some advantages compared to the “normal structure” described before: (1) The poly-Si film features a smooth surface and is directly accessible for subsequent process steps (e.g., epitaxial thickening). (2) The Al-rich layer between the poly-Si film and the glass substrate can be used as contact layer and back reflector in device configurations. The disadvantage is related to the fact that for the “inverse structure” all subsequent process steps are limited to the eutectic temperature of the Al/Si system (577^{o}C), to prevent the formation of a liquid phase.

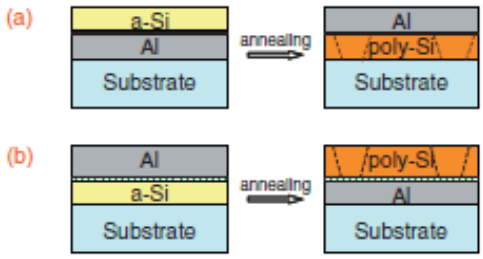

Fig.1.7 Structural difference between (a) conventional ALILE and (b) inverted-ALILE [37]

Therefore the Al-rich layer with optical reflectivity is substantially lower than an aluminum film. Light trapping is of crucial importance for crystalline silicon thin-film solar cells. An important component of any light trapping scheme for thin-film solar cells is an efficient back reflector layer. The back reflector layer expects to capable of high optical reflectance over a broad wavelength band. The back reflector can be increased the current of solar cells.

In the previous reports, few detailed study has been performed on inverted-ALILE. Furthermore, Al-rich layer by inverted-ALILE has never reported at all. In this study, inverted-ALILE process with Al-rich layer and inverted-ALILE process with crystallographic orientation are extensively studied and inverted-ALILE sample is applied to thin film silicon solar cell fabrication in order to prove the potential of inverted-ALILE for high current thin film silicon solar cells

1.5 Scope of this thesis

As discussed in Section 1.2, thin film silicon solar cells have a great potential for next

generation solar cells due to its low-coat, thin film availability and abundance of material. A drawback of thin film silicon solar cells as compared with wafer based c-Si solar cells is its low conversion efficiency. Thin film poly-Si solar cell with foreign substrates is one of the strong candidates for next generation solar cells, and ALILE is a quite promising process for large grained poly-Si thin film, which has possibility of realizing high efficiency thin film solar cells. However, an inevitable problem in association with solar cell structure exists in solar cells with ALILE sample as discussed in section 1.3.4. In order to overcome the structural drawback of ALILE solar cells, inverted-ALILE was proposed by Kuraseko *et al*. The inverted-ALILE sample is studied method of forming Al-rich layer to thin film silicon solar cell fabrication in this study. Annealing of Al/a-Si/glass layers leads to the formation of an poly-Si/Al-rich/glass layers and the Al-rich layer acts as optical reflector as well as an electrical contact. Additional advantage is the absence of the removal process of the Al-rich layer in the ALILE process. However, it was found that the Al-rich layer after the inverted-ALILE process shows poor reflectivity with appreciable optical transmission of the films, which indicates the light leakage through defects (holes) in the Al-rich layer after annealing.[15)] In chapter 4, the mechanism of inhomogeneity in the inverted-ALILE process with defective Al-rich back reflector is investigated and its origin is discussed in terms of the impurity contained in the original amorphous silicon layer before crystallization.

In addition, the crystal orientation of the poly-Si layer is studied in chapter 3. Si(100) is essential for texturing antireflection structures and Si(111) is useful as epitaxial templates for advanced solar-cell materials. We report the comprehensive study of inverted-ALILE by focusing on effects of precursor Al thickness on crystal orientation

of poly-Si. The Al thickness controlled preferential orientation of (100) or (111) poly-Si and a model base on the phase transition of interfacial Al oxide are presented.

In chapter 2, experimental details are shown. Preparation methods of thin films are described. Annealing apparatus and basic annealing conditions are also shown. Characterization techniques of structural and electrical properties employed in this study are detailed.

In chapter 3, the thickness-modulated inverted-ALILE crystallization technique enables to control the orientation of polycrystalline Si films on glass substrates. The (111) –orientation fraction reached 94.8% for the 45nm-thick sample. This mechanism was discussed in terms of the heterogeneous nucleation energy.

In chapter 4, requirements for the realization of inverted-ALILE process, which means the formation of both large-grained poly-Si layer and aluminum-rich bottom layer on glass substrate, are discussed. Influence of impurity in precursor a-Si sample is also demonstrated.

In chapter 5, inverted-ALILE samples are applied to thin film silicon solar cells fabrication. Fabrication procedure of solar cells using inverted-ALILE samples is given and solar cell performance of inverted-ALILE solar cell is demonstrated. Challenges remaining in inverted-ALILE solar cells are discussed.

In the final chapter, conclusions obtained through this work are summarized.

1.6 References

1. PV News & RTS Corporation report, 2011.

2. A. Wang, J. Zhao, S.R. Wenham and M.A. Green: Progr. Photovoltaics Res. Appl, **4**

(1996) 55.

3. W. Shockley and H. J. Queisser: J. Appl. Phys, **32**(1961) 510

4. M. A. Green: Physica E, **14** (2002) 65.

5. T. Takagi, M. Ueda, N. Ito, Y. Watabe, H. Sato, and K. Sawaya: Thin Solid Films **502** (2006) 50.

6. M. A. Green, K. Emery, Y. Hishikawa, W. Warta: Progr. Photovoltaics Res. Appl, **17** (2009) 85.

7. Susumu Fukuda et al: in Proceedings of the 21st European Photovoltaic Solar Energy Conference, Dresden, Germany, September **4**, (2011), p. 1535.

8. C. Spinella, S. Lombardo, F. Priolo: J. Appl. Phys, **84** (1998) 5383

9. M. J. Keevers, T. L. Young, U. Schbert, M. A. Green: in *Proceedings of the 22nd European Photovoltaic Solar Energy Conference*, Milan, Italy, 3-7 (2007) p.1783.

10. N. H. Nickel, Laser Crystallization of Silicon (Semiconductors and Semimetals 75), (Elsevier, Amsterdam, 2003)

11. S. R. Herd, P. Chaudhari, M. H. Brodsky: J. Noncryst. Solids, **7** (1972) 309

12. G. Ottaviani, D.Sigurd, V. Marrello, J.W. Mayer, J.O. McCaldin: J. Appl.Phys, **45** (1974) 1730.

13. G. Majni, G. Ottaviani: Appl. Phys. Lett, **31** (1977) 125.

14. G. Ottaviani, G. Majni: J. Appl. Phys, **50** (1979) 6865.

15. L.M. Koschier, S.R. Wenham, M. Gross, T. Puzzer, A.B. Sproul, in *Proceedings of the 2nd World Conference on Photovoltaic Energy Conversion*, 6–10 (1998) 1539.

16. O. Nast, T. Puzzer. L.M.Koschier, A.B. Sproul, S.R. Wenham: Appl. Phys. Lett, **73** (1998) 3214.

17. O. Nast, S. Brehme, D.H. Neuhaus, S.R.Wenham: IEEE Trans. Electron Devices **46**

(1999) 2062.

18. O. Nast, S.R. Wenham: J. Appl. Phys, **88** (2000) 124.

19. O. Nast, A.J. Hartmann: J. Appl. Phys, **88** (2000) 716.

20. S. Gall, I. Sieber, M. Muske, O. Nast, W. Fuhs, in *Proceedings of the 17th European Photovoltaic Solar Energy Conference*, Munich, Germany, 22–26 October 2001 (2002) 1846.

21. E. Pihan, A. Slaoui, P. Roca i Cabarrocas, A. Focsa: Thin Solid Films, **451** (2004) 328.

22. P.I.Widenborg, A.G. Aberle: J. Cryst. Growth, **242** (2002) 270.

23. S.Gall, J. Schneider, J. Klein, M. Muske, B. Rau, E. Conrad, I. Sieber, W. Fuhs, D. Van Gestel, I. Gordon, K. Van Nieuwenhuysen, L. Carnel, G. Beaucarne, J. Poortmans, M. St¨oger-Pollach, P. Schattschneider, in *Proceedings of the 31st IEEE Photovoltaic Specialists Conference*, Lake Buena Vista (FL), USA, 3–7 January 2005, p. 975.

24. K.Y. Lee, M. Muske, I. Gordon, M. Berginski, J. D'Haen, J. H¨upkes, S. Gall, B. Rech: Thin Solid Films **516** (2008) 6869.

25. J. Schneider, A. Schneider, A. Sarikov, J. Klein, M. Muske, S. Gall, W. Fuhs: J. Noncryst. Solids, **352** (2006) 972.

26. A. Sarikov, J. Schneider, M. Muske, I. Sieber, S. Gall, Thin Solid Films **515** (2007) 7465

27. B. Rau, E. Conrad, and S. Gall, 21EUPVSEC (2006) 1418

28. I. Gordon, L. Carnel, D. Van Nieuwenhuysen, G. Beaucarne, J. Poortmans, Thin Solid Films **487** (2005) 113.

29. D. Van Gestel, I. Gordon, L. Carnel, K. Van Nieuwenhuysen, G. Beaucarne,

J. Poortmans, in *Technical Digest of the 15th International Photovoltaic Science and Engineering Conference*, Shanghai, China, 10–15 October 2005, p. 853.

30. S. Gall, C. Becker, E. Conrad, P. Dogan, F. Fenkse, B. Gorka, K.Y. Lee, B. Rau, F. Ruske, B. Rech: Solar Energy Mater. Solar Cells, **93** (2009) 1004.

31. O. T¨uz¨un, A. Slaoui, I. Gordon, A. Focsa, D. Ballutaud, G. Beaucarne, J. Poortmans: Thin Solid Films, **516** (2008) 6892.

32. D. Dimova-Malinovska, O. Angelov, M. Kamenova, A. Vaseashta, J.C. Pivin: J. Optoelectron. Adv. Mater, **9** (2007) 355.

33. K.Y. Lee, C. Becker, M. Muske, F. Ruske, S. Gall, B. Rech, Appl. Phys. Lett. **91** (2007) 241911.

34. G. Ekanayake, H.S. Reehal: Vacuum **81**(2006) 272.

35. G. Ekanayake, T. Quinn, H.S. Reehal: J. Cryst. Growth, **293** (2006) 351

36. J.H. Kim, J.Y. Lee, Jpn. J. Appl. Phys, **35** (1996) 2052.

37. H. Kuraseko, N. Orita, H. Koaizawa, M. Kondo, Appl. Phys. Express **2** (2009) 015501.

Chapter 2

Experimental details

2.1 Preparation of thin films

2.1.1 Deposition of silicon thin films for inverted-ALILE process

Amorphous silicon films, which were employed in precursor sample of inverted-ALILE, were deposited by sputtering system and plasma-enhanced chemical vapor deposition (PECVD) system.

2.1.1.1 Sputtering system

Sputtering was employed for prepared a-Si on glass substrate. The chamber pressure during a-Si deposition was kept constant at 0.5 Pa with Ar flow rate of 10sccm. Radio frequency (RF) of 200W was applied. The system was evacuated using turbo-molecular pump to a background pressure of approx. 3.2×10^{-4}Pa, 1.2×10^{-2}Pa. In case of the high background pressure(1.2×10^{-2}Pa), sputtering chamber was exposed to air in 30min.

2.1.1.2 Plasma-enhanced chemical vapor deposition (PECVD) system

The deposition system consists of gas source system, deposition chamber and gas exhaust system. As a source gas, SiH_4, H_2 and PH_3 were used in this study. Gases were introduced into the deposition chamber through a mass flow controller. Deposition chamber was equipped with two parallel electrodes. Precursor a-Si films of inverted-ALILE sample were prepared with the deposition conditions shown in Table 2.1

Table 2.1 Deposition conditions of a-Si film for inverted-ALILE precursor sample.

Flow rate	SiH_4	300sccm
Pressure		40Pa
Substrate temperature		180°C
RF power		110W
Deposition rate		0.49nm/s

2.1.2 Deposition of aluminum films for inverted-ALILE process

Aluminum films were deposited using vacuum evaporation system in this study. As an evaporation source, 25mm of Al wire (purity of 99.99%) was set tungsten wire. The chamber was pumped down with a turbo molecular pump, and the base pressure inside the chamber was below 1×10^{-6} Torr. Input power was kept constant at 30 A, and the deposition was the deposition was carried out without intentional heating of substrates. Deposition rate was 0.6nm/s.

2.1.3Deposition of TCO and Ag for solar cells

Sputtering was employed for preparing TCO and Ag electrodes. Indium tin oxide (ITO) film was sputtered as a TCO electrode on solar cells and Ag grid electrode was used to compensate poor conductivity of TCO. Ar gas was employed as a process gas of the sputtering. RF of 100W was used for ITO deposition and direct current (DC) of 100W for Ag deposition, respectively. No additional heating of substrates was carried out. Deposition rate of ITO film and Ag film was 0.11 nm/s and 0.67 nm/s, respectively.

2.1.4 Substrate

Corning 1737 glass was used as a cost effective, alkali-free glass substrate. Strain point is 666 ^{o}C. Substrate thickness was 1.1nm. Before deposition, substrates were carefully cleaned by ultrasonic with chemical cleaning solution and de-ionized water at15min every process.

2.2Annealing apparatus and procedure

The prepared sample was cut by 2.5cm×2.5cm and placed on the heating stage in the annealing chamber. During the annealing, 2.0 SLM of N_2 gas was flowed in the chamber to avoid oxidation of the sample. The pressure in the chamber was atmospheric pressure. Temperature of the heating stage was measured with a thermocouple and was precisely controlled by changing input power to the heater mounted inside the heating stage. Figure.2.1 incidents an example of temperature profile of the heating stage from

room temperature to a set temperature (450 °C). The temperature of the heating stage reached the set temperature in ~ 30 min.

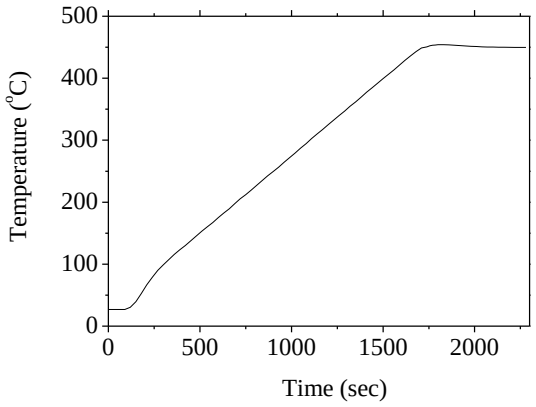

Fig.2.1 A temperature profile of the heating stage

2.3 Characterization techniques

2.3.1 Optical microscope

An optical microscope (KEYENCE) was employed for in-situ observation of layer exchange process during annealing. The annealing system was equipped with the microscope. Camera images could be observed in-site at a monitor and recorded with typical time intervals depending on the process parameters. The spatial resolution limit of the setup was 200nm. Evolution of silicon growth was clearly observed as shown in Fig.2.2. In the images obtained, brighter area indicates the existence of aluminum, which possesses higher reflectance in the range of visible light than that of silicon. Red area demonstrates silicon grains.

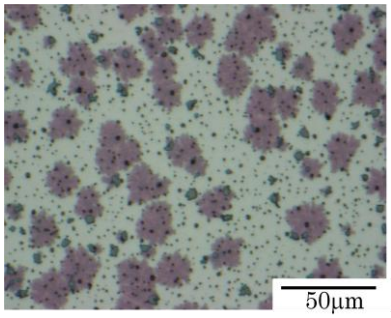

Fig.2.2 An image obtained with optical microscope during annealing

2.3.2 Ultraviolet-visible spectrophotometer

Ultraviolet-visible spectrophotometer is the quantitative measurement of the reflection and transmission properties of a material as a function of wavelength. They can also be designed to measure the diffusivity on any of the listed light ranges that usually cover around 175nm-3300nm using different controls and calibrations. Two radiation sources, a deuterium lamp and halogen lamp, cover the working wavelength range of the spectrometer. Deuterium lamps emit an almost continuous spectrum of light ranging from the main UV wavelengths of 175-400nm to the visible spectral range. Halogen lamps product a continuous spectrum of light, from near ultraviolet to deep into the infrared(350nm-3300nm). Spectrophotometer generally uses a diffraction grating, a collimator, a movable slit, and a photodetector. The broad band illumination source is aimed at the entrance slit. The slit is placed at the effective focus of a curved mirror (the collimator) so that the light from the slit reflected from the mirror is collimated. The collimated light is diffracted from the grating and then dispersed on the exit silt. At the exit slit, the colors of the light are spread out. The range of color leaving the exit slit is a function of the width of the slits. The light enters at a photomultiplier in integrating

sphere. Photomultiplier produces a small current even at the dark current. Spectrophotometer generally demand photomultipliers designed to minimize dark current. Transmittance and reflectance were measured by Lambda 950 UV/Vis/NIR Spectrophotometer. This machine features an all-reflecting, double-monochromator optical system.

2.3.3 Energy dispersive X-ray spectrometry (EDX)

Energy dispersive X-ray spectrometry (EDX) is an analytical technique used conjunction with scanning electron microscopy (SEM). It relies on the investigation of an interaction of some source of X-ray excitation and a sample. To stimulate the emission of characteristic X-rays from a specimen, a high-energy beam of charge particles such as electron, is focused into the sample being studied. The incident beam may excite an electron in an inner shell, ejecting from the shell while creating an electron hole where the electron was. An electron from an outer, higher-energy shell then fills the hole, and the difference in energy between the higher-energy shell and the lower energy shell may be released in the form of an X-ray. The number and energy of the X-rays emitted form a specimen can be measured by an energy-dispersive spectrometer. As the energy of the X-rays is characteristic of the difference in energy between the two shells, and of atomic structure of the element form which they were emitted, this allows the elemental composition of the specimen to be measured.

The penetration depth of the electron is increased at high energy-electron. This phenomenon is described with the equation as below:[1]

$$R = \frac{27.6 \times E_0^{1.67} A}{\rho Z^{8/9}} \qquad \text{(Eq. 2.1)}$$

Where R is the penetration depth of the electron, E_0 is energy of the incident electron, A is atomic number, Z is the Avogadro constant, ρ is the density. Within Eq.2.1 R can be determined if E_0 is constant.

In this study, JEOL JED-2300T was employed with EDX system. While analyzed by EDX, beam spot size was at 1.0nmϕ.

2.3.4 Electron backscatter diffraction (EBSD)

Electron backscatter diffraction (EBSD) is the technique by which a scanning electron microscope (SEM) can be used to evaluate the microstructure of a sample based on crystallographic analysis. The electron beam detects the backscattered electrons with phosphor screen. The incident angle of the electron beam from the sample surface is 20^o. The penetration depth of the electron is decreased and the fraction of backscattered electrons from the sample is increased.

Bragg's condition:

$$n\lambda = 2d\sin\theta \qquad \text{(Eq. 2.2)}$$

Where n is an integer, λ is the wavelength of the electron beam, *d* is the lattice spacing and θ is the diffraction angle.

Theoretically, the maximum resolution, d, that one can obtain with microscope has been limited by the wavelength of the photons that are being used to probe the sample,

λ and the numerical aperture of the system. Like all matter, electrons have both wave and particle properties, and their wave-like properties mean that a beam of electrons can be made to behave like a beam of electromagnetic radiation. The wavelength of electrons is

$$\lambda = \frac{h}{\sqrt{2m_0 E\left(1+\frac{E}{2m_0 c^2}\right)}} \qquad \text{(Eq. 2.3)}$$

Where, h is Plank's constant, m_0 is the rest mass of an electron and E is the energy of the accelerated electron. Electrons are usually generated in an electron microscope by a process known as thermonic emission from a filament, alternatively by field electron emission. The electrons are the accelerated by an electric potential (measured in volts) and focused by electrostatic and electromagnetic lenses onto the sample. The electron is formed when many different planes diffract different electrons to form Kikuchi bands which correspond to each of the lattice diffracting planes. (Fig.2.3) Each band can be indexed individually by the Miller indices of the diffracting plane which formed it.

$$w = \frac{1}{d} = \frac{1}{a}\sqrt{h^2+k^2+l^2} \qquad \text{(Eq. 2.4)}$$

Where, h,k,l is the Miller indices, a is lattice constant.

In this study, Oxford instruments HKL Channel 5 was employed with SEM system of Hitachi high-technologies S-4300. While analyzed by EBSD, magnification of the sample image was constant at x1,500.

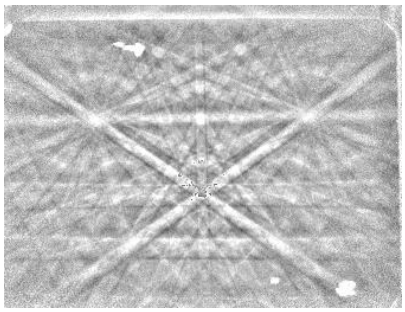

Fig.2.3 A electron backscatter diffraction pattern of polycrystalline silicon by inverted-ALILE, taken at 20kV with a field-emission electron source.

2.3.5 Transmission electron microscope (TEM)

Transmittance electron microscope (TEM) is an analytical tool that allows detailed micro-structural examination through high-resolution and high-magnification imaging. TEM is an electro-optical microscope which uses electromagnetic lenses to focus and direct an electron beam. Data is collected from the beam after it passes through the sample. The transmitted beam contains information about electron density, phase and periodicity; this beam is used to form an image. For thin crystalline samples, this produces an image that consists of a pattern of dots in the case of a single crystal, or a series of rings in the case of a polycrystalline or amorphous solid material. For the single crystal case the diffraction pattern is dependent upon the orientation of the specimen and the structure of the sample illuminated by the electron beam. Fig.2.4 provides the investigator with information about the space group symmetries in the crystal and the crystal's orientation to the beam path. TEM specimens are requires to be at most hundreds of nanometers thick. High quality samples will have a thickness that is comparable to the mean free path of the electrons that travel through the samples, which

may be only a few tens of nanometers. Focused ion beam (FIB) methods have been used to prepare samples. FIB is destructive to the specimen. When the high-energy gallium ions strike the sample, they will sputter atoms from the surface. Gallium atoms will also be implanted into the top few nanometers of the surface, and the surface will be made amorphous. Because of the sputtering capability, the FIB is used as a nano-machining tool, to modify or machine materials at nanoscale. Commonly the smallest beam size for imaging is 2.5-6nm. The smallest milled features are somewhat larger (10-15nm) as this is dependent on the beam size and interaction with the sample being milled. Cross-sectional image view images were observed by Hitachi H-9000UHR operated at an accelerate voltage of 300kV. Selected area electron diffraction (SAED) images were also observed by the same system. The camera length was 1.0nm and the selected area is ~100nmφ.

Fig.2.4 Crystalline diffraction pattern form a grain of FCC Aluminum

2.3.6 Secondary ion mass spectrometry (SIMS)

Secondary ion mass spectrometry is a technique used to analyze the composition of thin films by sputtering the surface of the specimen with a focused primary ion beam and collecting and analyzing ejected secondary ions. Three basic types of ion guns are

employed. In one, ions of gaseous elements are usually generated by electron ionization, for instance Ar^+ gas or O_2^+. A second source type, the surface ionization source, generates Cs^+ primary ions. Cesium atoms vaporize through a porous tungsten plug and are ionized during evaporation. A third source type, a liquid metal ion gun is liquid at room temperature. The choice of the ion species and ion gun respectively depends on the required current, the required beam dimensions of the primary ion beam and on the sample which is to be analyzed. Oxygen primary ions are often used to investigate electropositive elements due to an increase of the generation probability of positive secondary ions, while cesium primary ions often are used when electronegative elements are being investigated. For short pulsed ion beams in static SIMS, the liquid metal ion gun is most often deployed for analysis. They can be combined with either an oxygen gun or a cesium gun during element depth profiling.

In this study, SIMS analysis was carried out with CAMECA IMS-6f system using. While analyzed by EBSD, magnification of the sample image was constant at x1,500.

2.3.7 I-V characteristics

The most important parameter defining the quality of a solar cell is its conversion efficiency, η. Conversion efficiency is defined as the ratio of electrical output power to the optical input power. Since the output power is dependent of the load, the maximum power point (with optimized load) of output can be used for determining the conversion efficiency. Figure.2.5 shows schematic current-voltage characteristic of a solar cell under illumination. Three parameters define the performance of a solar cell under illumination: the open circuit voltage (Voc), the short circuit current (Jsc) and the fill

factor (FF). Voc and Jsc are the values of voltage and current obtained under at the maximum point. The current-voltage (I-V) characteristic of the device is given by:

$$J(V) = J_{sc} - J_0 \left[\exp\left(\frac{qV}{nkT}\right) - 1\right] \quad \text{(Eq. 2.5)}$$

Where J(V) is the current J at voltage V, J_0 is the reverse saturation current, q is the electronic charge, n is the diode factor, k is Boltzmann constant, T is the temperature and J_{sc} is the short circuit current. Under open circuit conditions, J=0 and

$$Voc = \frac{nkT}{q} \ln\left(\frac{J_{sc}}{J_0} + 1\right) \quad \text{(Eq. 2.6)}$$

The cell power density is given by $P=J \cdot V$. P reaches a maximum at a voltage V_{op} with a corresponding current desity of J_{op}, as shown in Fig.2.5. The optimum load thus has a resistance given by V_{op}/J_{op}, The fill factor is defined as $FF= JopVop/JscVoc$. The efficiency η of the solar cell is the power density delivered at operating point as a fraction of the incident light power density, P_{in}:

$$\eta = \frac{J_{op} \cdot V_{op}}{P_{in}} \times 100 = \frac{J_{sc} \cdot V_{oc}}{P_{in}} \times 100 \quad \text{(Eq. 2.7)}$$

In this study, solar cells were characterized by current-voltage under standard air mass 1.5 (AM 1.5) illumination.

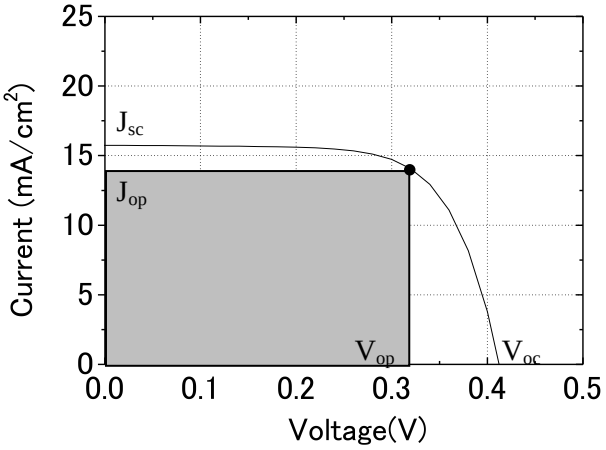

Fig.2.5 A schematic graph of current-voltage curve.

2.3.8 Quantum efficiency (QE)

The specimen dependence of a solar cell is characterized by its quantum efficiency. The photocurrent generated by a solar cell under illumination at short circuit depends on the incident light. To relate the photocurrent density, Jsc, to the incident spectrum we need to know the quantum efficiency (QE) of the solar cell. QE is the probability that an incident photon of energy delivers one electron to the external circuit. Therefore,

$$J_{sc} = q \int_0^{\infty} I(\lambda) QE(\lambda) d\lambda \qquad \text{(Eq. 2.8)}$$

Where I(E) is the incident spectral photon flux density, the number of photons of energy in the range of λ to $\lambda+d\lambda$ which are incident on unit area in unit time and q is the electronic charge. There are two different definitions for QE, that is, internal quantum efficiency (QE_{in}) and external quantum efficiency (QE_{out}). Reflection of the incident

light on the front surface was taking into consideration in the internal quantum efficiency. However, reflection was neglected in the latter case.

Relationship between two definitions can be written as

$$QE_{in}(\lambda) = \frac{QE_{ext}(\lambda)}{1-R(\lambda)} \quad \text{(Eq. 2.9)}$$

In this study, external quantum efficiency was measured. QE depends on the following factors:

· the absorption of the incident light in the absorber material

· efficiency of charge separation and collection

The absorption of the incident light in the absorber material depends on the absorption coefficient of the absorber material, absorption at the p-layer or front TCO, and texturing effect. Efficiency of charge separation and collection is dependent on the built-in potential in the intrinsic layer and the recombination rate of the carrier and so on.

2.4 Reference

[1]K. Kanaya and S. Okayama, J. Phys. D. Appl. Phys, 5, 43-58 (1972).

Chapter 3

Influence of oxygen on the orientation control in Inverted-ALILE

3.1 Introduction

In this chapter, requirement for the realization of inverted-ALILE process, which means the formation of large-grained poly-Si layer is discussed. Important condition for successful inverted-ALILE process is demonstrated in this study. Influence of the ratio of a-Si layer thickness to aluminum layer on the obtained inverted-ALILE sample properties is discussed. Also thickness of Al layer in the precursor sample of inverted-ALILE is focused. In particular, influence of the oxide layer on Al layer used inverted-ALILE sample properties is discussed.

3.2 The ratio of a-Si layer thickness to aluminum film

The ratio of a-Si thickness to aluminum is one of the essential parameter for inverted-ALILE. In case of conventional ALILE process, it was reported that an oxidized aluminum interlayer remains at the same during annealing and thickness of the obtained poly-Si film depends on the distance between glass substrate and interlayer, initial aluminum layer thickness [1]. It was also described that excess a-Si was needed to form a continuous uniform poly-Si film. In the case of conventional ALILE, a

continuous poly-Si is the only requirement for ALILE process. In contrast, in the case of inverted-ALILE, not only a continuous uniform poly-Si but also an aluminum-rich metallic layer is required. The obtained poly-Si is employed as p+-layer of p-i-n solar cell. Aluminum-rich metallic layer formed between the poly-Si and glass substrate can be employed as a bottom electrode and as a reflecting layer. As a bottom electrode, lower sheet resistance is needed. Higher reflectance in the visible light range is expected as a reflecting layer. In this section, samples with three different ratio of a-Si thickness to aluminum were prepared and inverted-ALILE samples were evaluated. Structural parameters of precursor sample are summarized in Table 3.1. Three types of precursor samples were prepared; sample #1 : a-Si/Al=1:1; sample #2: a-Si/Al=1:0.8; sample #3: a-Si/Al=1:0.66. Native oxidized aluminum interlayer was employed in this study. Thickness of the interlayer was fixed at 13nm and air exposure time was1h.

Table 3.1 Deposition conditions of a-Si film for inverted-ALILE precursor sample.

Sample A		#1	#2	#3
a-Si/Al		1:1	0.8:1	0.66:1
Thickness (nm)	a-Si	200	250	300
	Al	200	200	200

Figure 3.1 shows direct mapping of intensity of Al related signals in the EDX spectra results. It can be observed that crystallization rate was almost independent of the ratio of a-Si thickness to aluminum. Darker area of the mapping indicates the formation of poly-Si and brighter area shows the aluminum remaining at the surface of the sample. As can be seen in the mapping of sample #3, the sample surface was fully covered with

poly-Si after annealing after 24 hour annealing. In contrast, in the case of sample #1 and sample #2, these samples surface were not fully covered with the resulting poly-Si and a portion of initial aluminum remained at the sample surface. In other words, a continuous uniform poly-Si layer could not be formed at these samples surface with precursor structure of a-Si/Al=1/1 and a-Si/Al=1:0.8. The volume of initial aluminum layer was almost the same with that of initial a-Si layer so that initial aluminum could not be excluded from the top layer with a diffusion of silicon. If p-i-n structure solar cells were fabricated with the sample #1 and sample #2, the obtained solar cells would indicate quite-low conversion efficiency due to the existence of shunt path between the bottom electrode (aluminum-rich metallic layer formed by inverted-ALILE process) and an absorber layer prepared on the inverted-ALILE sample. Therefore, sample #1 and sample #2 seem to be insufficient to inverted-ALILE process from the viewpoint of the formation of a continuous uniform poly-Si layer. Also, sample #3 seems to irreproducibility to inverted-ALILE process from the viewpoint of the formation of a continuous uniform poly-Si layer. Therefore, precursor sample was employed a-Si/Al=1:0.5 in this study. These structural parameters of precursor sample have reproducibility.

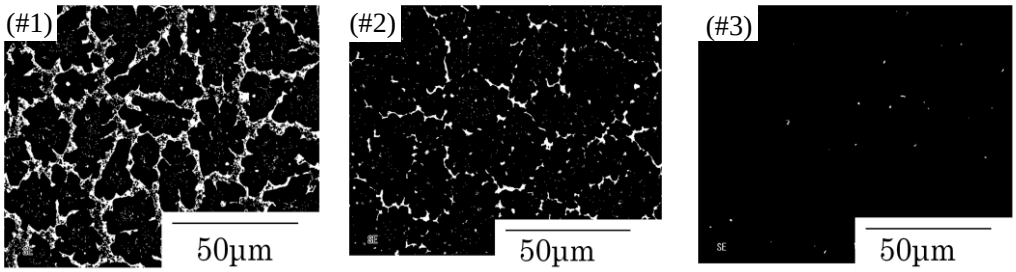

Fig.3.1 Direct mapping of intensity of Al related signals in the EDX spectra obtained from Sample A with different ratio of film thickness in as-annealed states. a-Si/Al = (#1)

1:1, (#2) 0.8:1, and (#3) 0.66:1.

3.3 The Al/Si thickness dependent ALILE process

a-Si films were prepared (thickness: 50-400nm) on SiO_2 glass substrates. Structural parameters of precursor sample are summarized in Table 3.2. Subsequently, a 13nm of aluminum thin film was deposited and exposed to ambient air for 1h in order to form AlOx membranes as diffusion control layers. After that, Al films were prepared with 45nm on the a-Si films. Finally, these samples were annealed at 450^{o}C for 6h in N_2 ambient. The crystal orientations of the grown Si films were evaluated by electron backscattering diffraction (EBSD) measurements.

Table 3.2 Deposition conditions of a-Si film for inverted-ALILE precursor sample.

Sample A				
a-Si/Al		0.5:1	0.5:1	0.5:1
Thickness (nm)	a-Si	90	120	400
	Al	45	60	200

The crystal orientations were evaluated using EBSD measurements. Fig. 3.2 shows the Al/Si thickness dependent crystal-orientation maps to the sample surfaces. The orientations in Fig.3.2 obviously depend on the Al/Si thickness: The [111]-orientation becomes dominant for the 45nm-thick sample; in contrast, the [100]-orientation for the samples with thick (>200nm) Al/Si layers.

The EBSD analysis derived the area-fraction of [100] and [111] orientations from the

orientation maps show in Fig. 3.2. The result is illustrated in Fig 3.3 as a function of the Al/Si thickness. Here, by definition, the [111] and [100] fraction s contains the orientations tilted within 20^{o} from the exact [111] and [100] orientations. The [111] fraction increases with decreasing the Al/Si thickness; in contrast, the [100] fraction increases with increasing the Al/Si thickness. Note that the [111] fraction reaches as high as 94.8% at the 45nm thickness, and the fraction reaches 84.9% at the 200nm thickness. These orientation fractions are the highest ever reported for the poly-Si layers on amorphous substrates. [11]

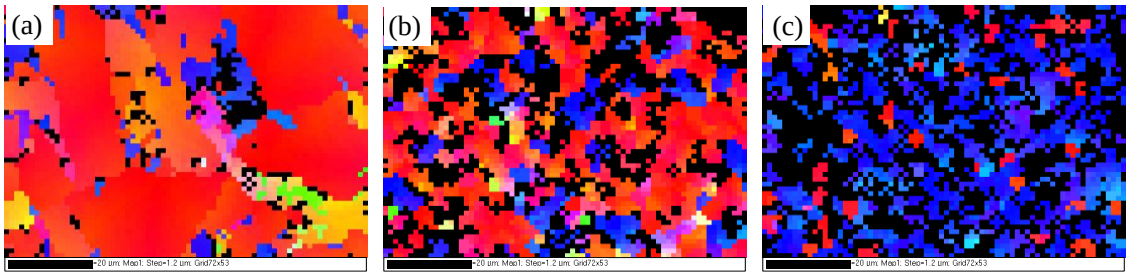

Fig.3.2 EBSD mapping of the grown Si layers surfaces with various thickness (45-200nm)

(poly-Si thickness, left: (a) 200nm; center: (b) 70nm; right:(c) 45nm)

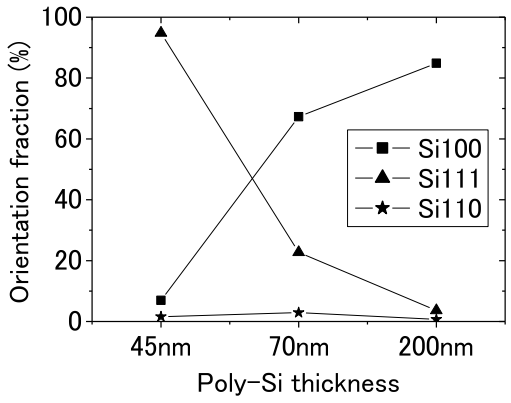

Fig.3.3 Al/Si thickness dependences of (111), (110) and (100) orientation fractions.

3.4 Crystallographic orientation of inverted-ALILE by interface impurities

The layer exchange process of sample A was performed at 450^{o}C for 15min at a-Si/Al =400nm/200nm. The annealed sample was taken out from the furnace. The EBSD was used to analyze the crystal orientation of the films. After EBSD observation at sample A annealing of 15min, inverted-ALILE sample with the annealing temperature of 450^{o}C was cleaned by wet etching, which resulted in the elimination of initial aluminum layer and native oxidized aluminum layer at the sample surface. Acid solution is the mixed solution containing phosphoric acid, nitric acid, acetic acid and dilution water with the volume ratio of 16:1:2:1, respectively (standard solution for aluminum etching).

The surface of the Al film is preferentially (111) orientated shown in Fig.3.4 (a). After wet etching of acid solution, the surface of the Si grains on the a-Si film are preferentially (100) orientated shown in Fig.3.4 (b). If a sample of Fig3.4 (a) is additionally annealed, the sample will indicate to crystal orientation as same as Fig.3.2 (a).

To understand the difference between Figure.3.2(a) and 3.4(a), Sawada et al. reported the lattice constant of γ-Al_2O_3(111) is close to that of Si(111) (mismatch:~2.4%),[9]. In addition, γ-Al_2O_3 is cubic crystal system, and Si(111) is same system too. Therefore, the orientation mapping are different to distinguish γ-Al_2O_3(111) from Si(111) by ESBSD measurements. This result clarified that the crystal orientation in Al by inverted-ALILE sample in initial step annealing, γ-Al_2O_3(111) is formed at the surface

of precursor Al layer. The γ-Al_2O_3(111) is formed by impurity from chamber inner wall.

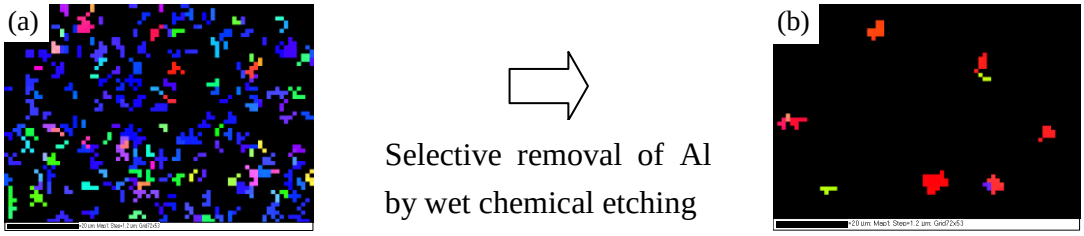

Figure.3.4 (a) EBSD image for sample A was taken out during crystal growth at 15min (b) EBSD image for (a) was etched off Al layer by acid solution.

3.5 Model of the inverted-ALILE process

Now this section is discussed the mechanism of the Al/Si thickness dependent inverted-ALILE process. Some paper on the ALILE describe that the Si nucleation heterogeneously occurs at the interface between Al and interfacial diffusion-controlling layers (AlOx layers in this experiment).

M. Kurosawa et al. measured statistical distributions of crystal orientation of Si grains obtained by AIC for samples with different air-exposure time (5min~24h). In the case of 5min, the fraction of (001) preferential orientation shows very high value (~80%). With increasing air-exposure time, the fraction of (001) orientation significantly decreases and the (111) fraction begins to increase. As a result, a very high fraction (~85%) of (111) orientation is obtained for the sample with air-exposure time 24h [12]. They discussed the interfacial Al oxide dependent AIC phenomena. The key issue to be considered is the phase transition of Al oxide during AIC process. Jeurgens *et al.* [13] reported that amorphous-Al_2O_3 membrane on Al films charge into γ-Al_2O_3 by solid-phase crystallization (SPC) at a temperature above 400^{o}C. Since (111) oriented Al

was used in the present experiments, the interfacial-oxide layers should change into (111)-oriented γ-Al_2O_3 layers by SPC at 450^{o}C for a certain annealing time. Schneider *et al*. calculated the free energy for Si nuclei generated at amorphous-Al_2O_3/Al interfaces as a function of nuclei orientation. Results indicated the lowest free energy for (001)-orientation, which could well explain that preferential (001)-orientation nuclei were obtained in the experiment. In the case of thin Al_2O_3 layers, i.e., short air exposure times, Si atoms can diffuse through the Al_2O_3 layers before the phase transition of Al_2O_3. Recently, Schneider et al. calculated the free energy for the Si nuclei generated at amorphous-Al_2O_3 interfaces as a function of nuclei orientation. Results indicated the lowest free energy for the (001)-orientation, which could well explain that the preferential (001)-oriented nuclei were obtained in the present experiment. [14].

The models of inverted-ALILE are schematically depicted in Fig.3.5. In the case of thick Al layer, it takes a certain time to diffuse Si atoms through the amorphous-Al_2O_3 layers. Then Si(111) crystals is difficult to grow on γ-Al_2O_3(111) membrane. Since precursor Al layer is thick, Si(100) crystals tends to grow on amorphous-Al_2O_3 membrane. In the case of thin Al layer, Si(100) crystals is difficult to grow on amorphous-Al_2O_3 membrane. Crystalline silicon is known to form preferentially (111) face [15], Si(111) crystals tends to grow on γ-Al_2O_3(111) membrane. Therefore, the Si(111) crystallization on γ-Al_2O_3(111) is dominated in precursor AlOx membrane.

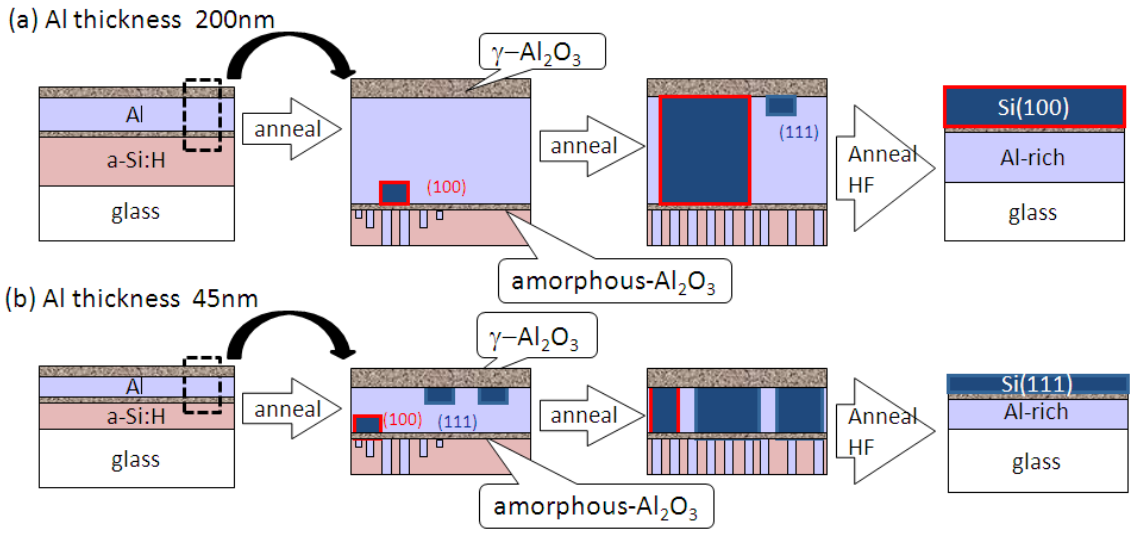

Fig.3.5 (a) Model for Si(100) nucleation (b) Si(111) nucleation for thin and thick precursor Al layers, respectively.

3.6 Summary

In this chapter, samples obtained by inverted-ALILE process were investigated the low-temperature (450^{o}C) focusing on the Al/Si thickness dependence. The crystal orientations of grown poly-Si on Al layers were controlled to (111) or (100) by modulating the Al/Si thickness. Namely, the (111)-orientation fraction reached as high as 94.8% for 45nm thick sample. In contrast, the (100)-orientation fraction reached 84.9% for the 200nm-thick sample. In addition, the qualitative model considering the formed of surface Al oxide layer is proposed. These poly-Si films with controlled-orientations promise to be favorable epitaxial templates for Si-based thin-film solar cells with texturing antireflection structure.

3.7 Reference

1. P. Campbell, S. R. Wenham, M. A. Green, *Sol. Energy Mater. Sol. Cells*, 31, 133, (1993).

2. D. Tsukada, Y. Matsumoto, R. Sakaki M. Takeishi, T. Saito N. Usami, T. Suemasu, T. Appl. Phys. Express **2**,051601, (2009).

3. S. Gall, J. Schneider, J. Klein, K. Hübener, M. Muske, B. Rau, E. Conrad, I. Sieber, K. Petter, K. Lips, M. Stöger-Pollach, P. Schattschneider, and W. Fuhs: Thin Solid Films **511** 7 (2006).

4. M. Jung, A. Okada, T. Saito, T. Suemasu, N. Usami, Appl. Phys. Express **3**, 095803, (2010).

5. M. Kurosawa, K. Toko, N. Kawabata, N. Kawabata, T. Sadoh, M. Miyao, Solid-State Electron, **60**, 7, (2011).

6. A. Okada, K. Toko, O. K. Hara N. Usami, T. Suemasu. *J. Cryst. Growth* **356**, 65 (2012).

7. O. Nast and S. R. Wenham, J. Appl. Phys. **88** 124 (2000)

8. M. Kurosawa, N. Kawabata, T. Sadoh, and M. Miyao: Appl. Phys. Lett. **95** 132103 (2009).

9. K. Sawada, M. Ishida, T. Nakamura, and N. Ohtake, Appl. Phys. Lett. **52**, 1672 (1988).

10. G. Ekanayake, T. Quinn, H.S. Reehal, J. Cryst. Growth **293**, 351 (2006).

11. O. Nast, A.J. Hartmann, J. Appl. Phys. **88**, 716 (2000).

12. M. Kurosawa, N. Kawabata, T. Sadoh, M. Miyao, Appl. Phys. Lett **95** 132103 (2009).

13. P. H. Jeurgens, W. G. Sloof, F. D. Tichelaar, and E. J. Mittemeijier, Thin Solid Films **418**, 89 (2002).

14. J. Schneider, A. Sarikov, J. Klein, M. Muske, I. Sieber, T. Quinn, H.S. Reehal, S. Gall and W. Fuhs, J. Cryst. Growth **287**, 423 (2006)

15. D. J. Eaglesham, A. E. White, L. C. Feldman, N. Moriya, and D. C. Jacobson, Appl. Phys. Lett. **70** , 1643 (1993).

Chapter 4

Impurity driven enhancement of homogeneity of inverted aluminum-induced layer exchange of silicon

4.1 Introduction

In this chapter, requirements for the realization of inverted-ALILE process, which means the formation of both large-grained poly-Si layer and aluminum-rich bottom layer on glass substrate, are discussed. Three important conditions for successful inverted-ALILE process are demonstrated in this study. a-Si layer in the precursor sample of inverted-ALILE is discussed. Influence of the impurity in a-Si layer on the obtained inverted-ALILE sample properties is discussed.

The mechanism of inhomogeneity in the inverted-ALILE process with defective Al back reflector is investigated and its origin is discussed in terms of the impurity contained in the original amorphous silicon layer before crystallization.

4.2 Inverted-ALILE samples preparation

The sample used consists of a Corning 1737 glass substrate, amorphous silicon layer at the bottom a thin alumina interlayer and an aluminum layer on the top. We have

prepared three different samples with amorphous silicon containing different amount of impurity. Sample a: Hydrogenated amorphous silicon (a-Si:H) layer was deposited using a PECVD method. The chamber pressure during a-Si:H deposition was kept constant at 40 Pa with SiH_4 flow rate of 300sccm. Radio frequency (RF) of 110W was applied. A substrate temperature was 180^{o}C and deposition rate was 0.49nm/s. Non hydrogenated amorphous silicon was deposited by a sputtering method. The deposition pressure was kept constant at 0.5 Pa with Ar flow rate of 10sccm. Two different sputtered samples were prepared under the background pressure of 3.2×10^{-4}Pa (Sample b)and 1.2×10^{-2}Pa (Sample c).

The thickness of the deposited Si film was 400 nm for all samples. In order to fabricate an oxidized Al membrane on the a-Si film, a thin Al film of 13nm was deposited on the a-Si film by vacuum evaporation and was naturally oxidized in air for an hour. During the air exposure, the sample temperature was kept at room temperature (RT). The naturally oxidized Al layer acts as a permeable membrane which can limit the mass transport of silicon and aluminum across the interface. Next, thicker Al layer (200 nm) was evaporated on the membrane layer. Finally, the samples were annealed in nitrogen atmosphere at 450˚C for 24 hours, and the polycrystalline silicon appears on the top with underlying aluminum-rich layer. Three different samples have been prepared by inverted-ALILE process containing different amount of impurity. Three different inverted-ALILE samples were prepared by Sample a, b and c of amorphous silicon. (Sample A by Sample a, Sample B by Sample b and Sample C by Sample c)

The optical reflectance of the crystallized film after layer exchange and underlying Al-rich layers were measured, separately. The reflectivity of Al-rich layers were measured after the top poly-Si films were removed by a reactive ion etching (RIE)

system (with SF_6:100sccm O_2:20sccm) for 10 min. Due to the low etching rate of aluminum layer, only the silicon layer can be selectively removed. To study the depth profile of aluminum across the entire layer, cross-sectional mapping of Al were measured by energy dispersive X-ray spectroscopy (EDX) for Samples A and C. Sample C was also observed by transmission electron microscopy (TEM). The depth profile of impurity concentration was measured by secondary-ion-mass spectroscopy (SIMS).

4.3 Inverted-ALILE using a-Si:H precursor with hydrogen

In order to observe the surface morphology of poly-Si film prepared at Sample A. Scanning electron microscope (SEM) was used to evaluate the surface morphology.

SEM micrograph in Fig.4.1 shows the surface of the Sample A after annealing. It shows that after inverted-ALILE processes, the samples surface was textured by irregularly-shaped nano-scale islands with various sizes.

The surface morphology of Sample A shows that micro-voids can easily be identified with Fig.4.1. The effused hydrogen leaves enhanced disorder and micro-voids in the a-Si:H precursor, which will stimulate dissolution of the Si atoms in Al and the consecutive re-arrangement into Si crystalline structure. The hydrogen effusion can create micro-voids in the poly-Si films. Grigorov et al show demonstrates micro-holes formed due to the effusion of hydrogen using ALILE sample. [1]

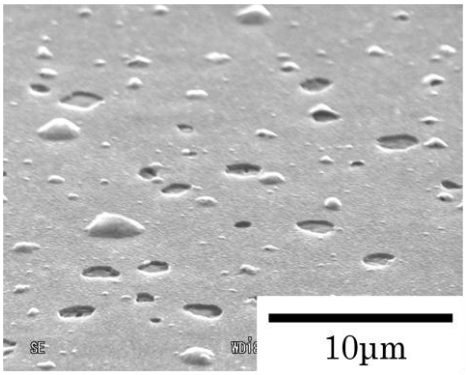

Fig4.1 SEM images of a poly-Si film obtained by inverted-ALILE of glass/a-Si:H (sample A) 400nm/Al 200nm at 450^{o}C : a-Si:H precursor layer hydrogen concentration)

The advantage of inverted-ALILE is to form a reflecting layer between glass substrate and poly-Si layer. Inverted-ALILE process is expected to form a final layer structure of glass/Al-rich/poly-Si from the precursor sample structure of glass a-Si/Al. The resulting aluminum-rich layer between glass substrate and obtained poly-Si layer is expected to act as a reflecting layer. Aluminum-rich layers formed by inverted-ALILE process with various a-Si are evaluated from the viewpoint of electrical sheet resistance and optical reflectance. Firstly, poly-Si layer fabricated at the sample surface by inverted-ALILE process was eliminated by using reactive ion etching (RIE). The source gas was a mixed gas of SF_6 and O_2, and the respective flow rate was 100 and 20SCCM. Pressure in the chamber was 20.0 Pa and RF power was100W. Etching time was 2min.

The reflectance is higher in the order of Sample A as shown in as show in Fig. 4.2. On the other hand, the transmittance is higher in the opposite order, Sample A as shown in Fig. 4.2. The reflectivity spectra show pronounced dip around 850nm for all the samples, which arises from inter-band transitions in Aluminum. [2] Reflectance of the obtained aluminum-rich layer was also measured by a spectrophotometer in the 300-1200 nm range. As shown in Fig. 4.2, a reflectance of ~60% was observed in all the range

measured in this study. A transmittance of ~20% was observed in all the range measured. From these results with regard to the aluminum-rich layer obtained by inverted-ALILE using a-Si:H precursor, the aluminum-rich layer is disadvantageous to use from the view point of the properties of aluminum-rich layer as a reflecting layer.

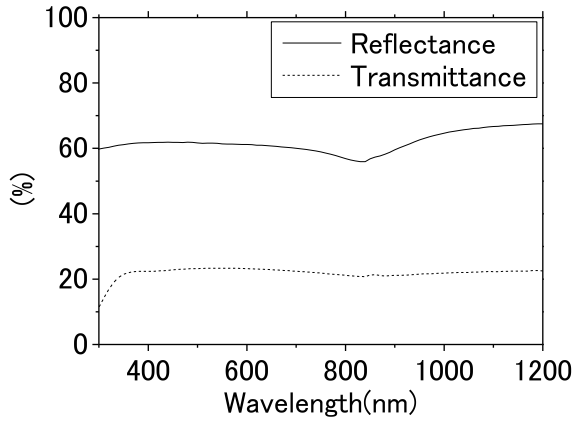

Fig.4.2 The optical reflection and transmission spectra, respectively, for Sample A after removing the polycrystalline silicon layer on the top.

4.4 Inverted-ALILE using a-Si precursor layer without hydrogen

Grigorov et al show observed when using precursor a-Si layers without hydrogen. The effusion can create micro-holes in the poly-Si films is not observed.

Inverted-ALILE sample using a-Si precursor was not observed the micro-holes in Fig.4.3.

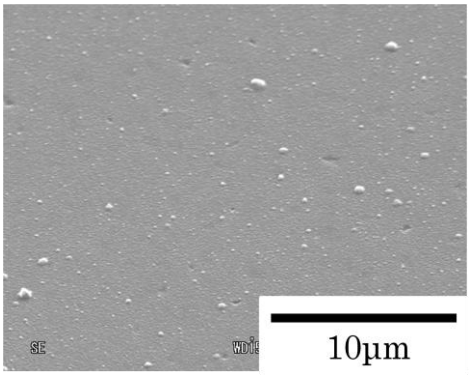

Fig4.3 SEM images of a poly-Si film obtained by inverted-ALILE of glass/a-Si (sample B) 400nm/Al 200nm at 450°C : a-Si precursor layer without hydrogen.

Figure 4.4 shows the optical reflection and transmission spectra, respectively, for different samples after removing the polycrystalline silicon layer on the top.

The reflectance is higher in the order of Sample B and A as shown in as show in Fig.4.4. On the other hand, the transmittance is higher in the opposite order, Sample A and B.

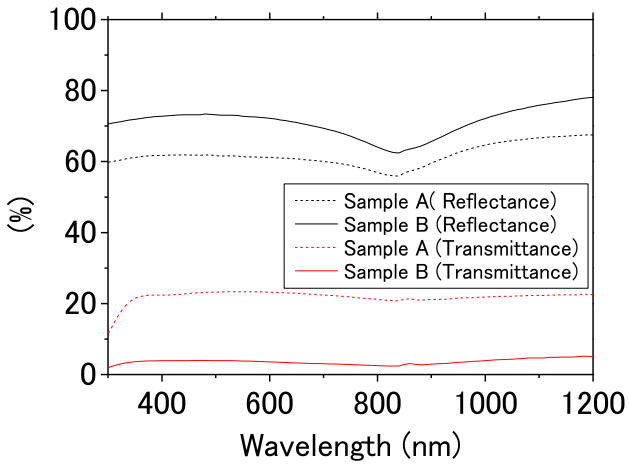

Fig.4.4 The optical reflection and transmission spectra, respectively, for Sample A and Sample B after removing the polycrystalline silicon layer on the top.

Figure 4.5 shows direct mapping of intensity of Al related signals in the EDX spectra obtained from Samples A and B in as-annealed states. The electron acceleration voltage was as low as 3.0 keV for the selective detection of elements near the sample surface. These results indicate that Sample A shows most inhomogeneous in-plain distribution of Al, while Sample B is more homogeneous than Sample A. The inhomogenerous contrast in Sample A is considered to arise from the presence of small Si crystallites within the newly evolved Al-rich layer as reported by Nast et al. for ALILE [3]. The origin of Si crystallites could be silicon that is not incorporated into the poly-Si layer. This is consistent with the optical reflection and transmission data in Fig.4.4.

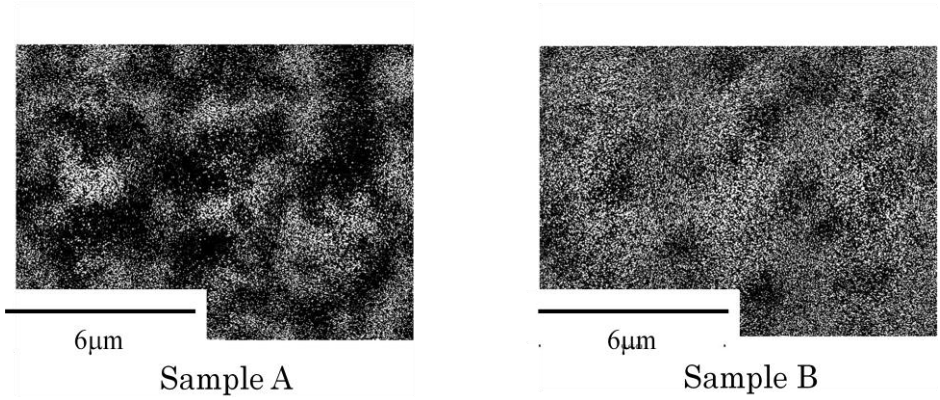

Fig.4.5 Direct mapping of intensity of Al related signals in the EDX spectra obtained from (1) Sample A and (2) Sample B.

Figure 4.6 shows the optical transmission for Sample A and Sample B after removing the polycrystalline silicon layer on the top in visible right range. There is variability among the reflectance reproducibility of Sample B and A. We are expected to replicate Al-rich layer of lower transmittance. This phenomenon is occurred when the sputtering

chamber was opened to change the target. We decide that water particles on the chamber wall are affect to forming Al-rich layer having high reflectance.

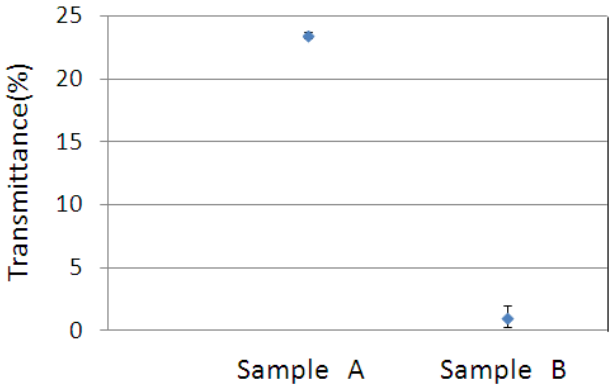

Fig.4.6 The optical transmission for Sample A and Sample B after removing the polycrystalline silicon layer on the top in visible right range.

4.5 Inverted-ALILE using a-Si precursor layer with impurity

Non hydrogenated amorphous silicon was deposited by a sputtering method. The deposition pressure was kept constant at 0.5 Pa with Ar flow rate of 10sccm. The precursor a-Si of Sample C was prepared under the background pressure of 1.2×10^{-2}Pa by sputtering machine. The base pressure is decreased after deposition in sputtering (1.2×10^{-2}Pa→2×10^{-3} Pa). The thickness of the deposited Si film was 400 nm for all samples. In order to fabricate an oxidized Al membrane on the a-Si film, a thin Al film of 13nm was deposited on the a-Si film by vacuum evaporation and was naturally oxidized in air for an hour. During the air exposure, the sample temperature was kept at room temperature (RT). The naturally oxidized Al layer acts as a permeable membrane which can limit the mass transport of silicon and aluminum across the interface. Next,

thicker Al layer (200 nm) was evaporated on the membrane layer. Finally, the samples were annealed in nitrogen atmosphere at 450˚C for 24 hours, and the polycrystalline silicon appears on the top with underlying aluminum-rich layer.

4.5.1 Surface morphology of the inverted-ALILE

In order to observe the surface morphology of poly-Si film prepared at Sample A, Sample B, Al film and Sample C. Four types of precursor samples were prepared; a-Si/Al=20nm/10nm, 40nm/20nm, 200nm/100nm and 400nm/200nm. Native oxidized aluminum interlayer was employed. Thickness of the interlayer was fixed at 13nm and air exposure time was 1h. Also Al film was evaporated on glass substrate at 10, 20, 100 and 200nm. This sample was annealed at 450^{o}C for 24h in a N_2 ambient. Scanning electron microscope (SEM) and atomic force microscope (AFM) were used to evaluate the surface morphology.

SEM micrographs in Fig.4.7 show the surface of the Sample A, Sample B and Sample C after annealing. It shows that after inverted-ALILE processes, the samples surface was textured by irregularly-shaped nano-scale islands with various sizes.

Fig.4.8 shows root mean square (RMS) of surface roughness versus the thickness of the grown poly-Si layer with Sample A, Sample B, Al(200nm) and Sample C. RMS of Sample B and Sample C is same as that of annealed aluminum film (200nm). However, RMS of Sample A is higher than that of other samples. Thick sample has especially high roughness. The RMS surface roughness increases with poly-Si thickness as shown in Fig.4.8. In addition, the surface roughness of Sample A is higher than that of Sample B and Sample C.

The surface morphology of Sample A shows that micro-voids can easily be identified with Fig.4.7 (a). The effusion of hydrogen during annealing could be suggested to be a reason for the difference in the structural properties of poly-Si, using a-Si and a-Si:H precursors. The effused hydrogen leaves enhanced disorder and micro-voids in the a-Si:H precursor, which will stimulate dissolution of the Si atoms in Al and the consecutive re-arrangement into Si crystalline structure. At higher hydrogen concentration in the precursor layers, the higher effused quantity of hydrogen will probably create conditions for an increased diffusion rate of Al in Si. Thus, the intermixing between Al and Si will take place within the bulk of the resulting poly-Si film. Additionally, the hydrogen effusion can create micro-voids in the poly-Si films. A SEM image of the surface of the poly-Si film obtained from precursor a-Si:H, prepared at 450^{o}C,as show in Fig.4.7(a). demonstrates micro-holes formed due to the effusion of hydrogen. Such a SEM image is not observed when using precursor a-Si layers without hydrogen. (Fig.4.7(b)-(c))

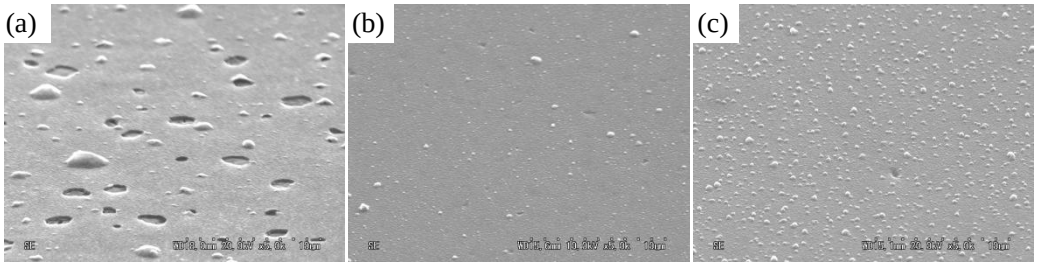

Fig.4.7 SEM images of a poly-Si film obtained by inverted-ALILE of glass/a-Si(sample A, B and C) 400nm/Al 200nm at 450^{o}C : (a)a-Si:H precursor layer hydrogen concentration); (b)a-Si precursor layer without hydrogen. (c) a-Si precursor with oxygen and hydrogen.

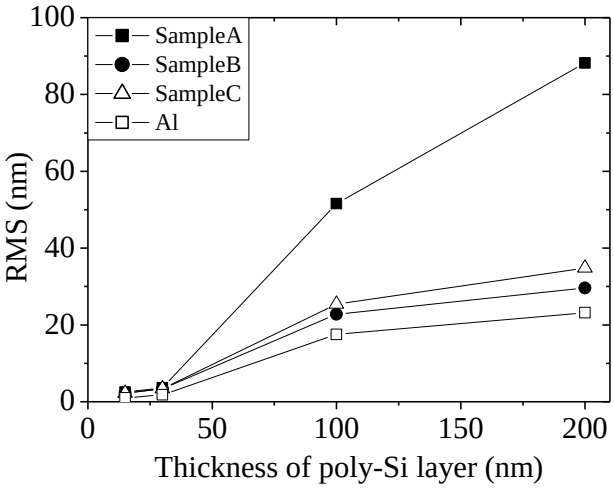

Fig.4.8 Root mean square(RMS) of surface roughness versus the thickness of the grown poly-Si layer with Sample A, Sample B, Al(200nm) and Sample C

4.5.2 Crystallographic orientation of poly-Si

It is well known that (100) crystallographic orientation is favorable for epitaxial growth of silicon with low temperatures. Lee at al. have succeeded the epitaxial growth of silicon with a thickness of 2μm by using ion beam sputter deposition (IBSD) at the deposition temperature of 325^{o}C [4]. Rau et al. have reported low-temperature epitaxial growth of silicon film on Si (100) wafer with a thickness of 2.5μm by using ECR-CVD at the temperature of 510^{o}C [5]. It was also experimentally confirmed that epitaxial growth occurred only at the beginning of the growth on Si (311) wafer, and Si (100) and Si (111) wafer offered no epitaxial growth of silicon. Platen *et al.* have investigated the possibility of epitaxial growth of silicon by using ECR-CVD with various substrate orientations, which resulted in $h_{epi}(100) >> h_{epi}(311) >> h_{epi}(111) >> h_{epi}(110)$ of h_{epi} as the thickness of epitaxial growth[6]. Considering these reports, Si (100) orientation has

a crucial advantage for epitaxial growth of silicon with low temperatures.

In general, X-ray diffraction analysis (XRD) and EBSD are employed as nondestructive analysis and SAED images of TEM analysis are used as destructive analysis when observing a crystallographic orientation of a matter. Among nondestructive methods, EBSD can observe, in principle, only the surface of the sample so that it is sufficient for this study. In this crystallographic orientation of the poly-Si film formed by inverted-ALILE sample was analyzed by using EBSD.

After annealing, inverted-ALILE sample with the annealing temperature of 450^{o}C was cleaned native oxidized aluminum layer and native oxidized silicon layer at the sample surface. The solution contains 2% hydrofluoric acid. The sample was treated with hydrofluoric acid solution for 1min, and rinsed with pure water and dried with N_2 gas.

Inverted-ALILE samples formed with three type a-Si were analyzed by EBSD. Figure 4.9, 4.10 and 4.11 shows the results of the analysis. We show orientation fraction of poly-Si in Fig.4.12. Each figure contains an inverse pole figure map and a band contrast map of the obtained poly-Si grains inverse pole figure map indicates a preferential orientation, and a band contrast map indicates sharpness of electron backscatter diffraction patterns. In a band contrast map, color area shows sharper patterns, which means high crystallinity with well-order crystals. In contrast, black area demonstrates having less sharper patterns, for example, at grain boundaries. Preferential (100) orientation is defined as the ratio of pixels in the orientation maps having an orientation within 20^{o} of (100) to the total number of pixels in the area under investigation[7]. Preferential (100) orientation was observed from all the inverted-ALILE samples in Fig.3.8. With sample A, Sample B and Sample C, 85.9%, 82.4% and 84.9% of the film surface area had a preferential (100) orientation. The preferential orientation of the

sample C shows a similar behavior compared to samples A and B.

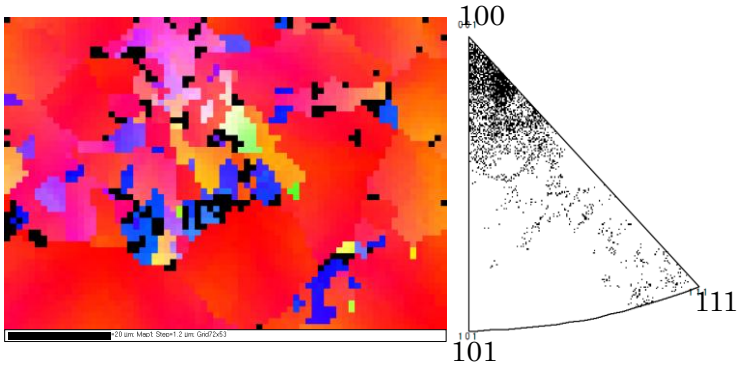

Fig.4.9 EBSD mapping (Sample A)

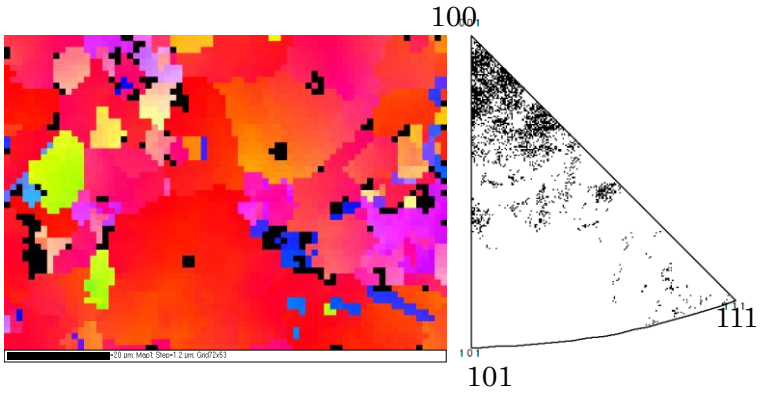

Fig.4.10 EBSD mapping (Sample B)

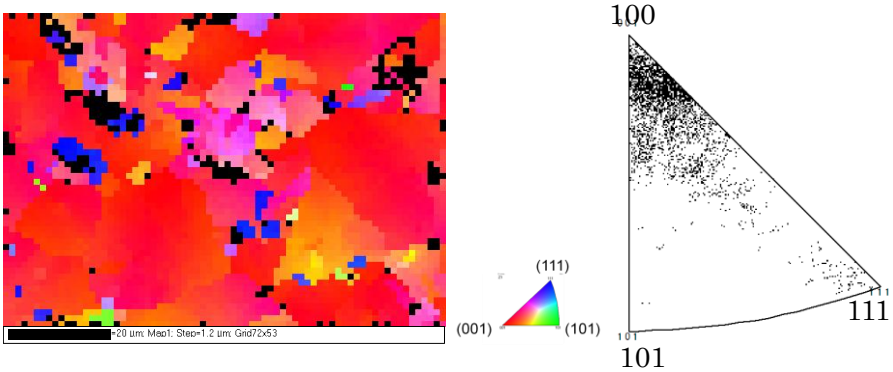

Fig.4.11 EBSD mapping (Sample C)

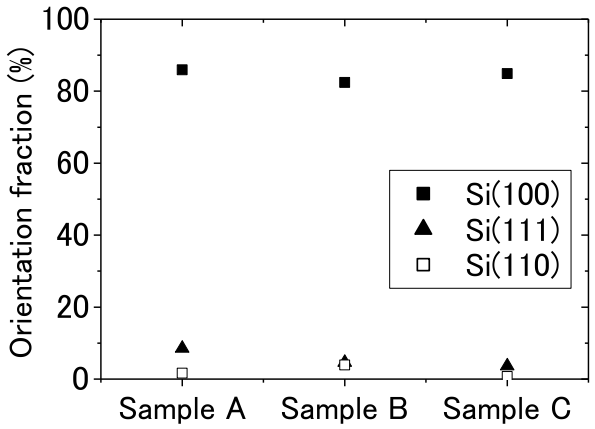

Fig.4.12 Orientation fraction of poly-Si

4.5.3 Electrical conductivity, reflection and transmission properties of Al-rich layers

Sheet resistance of the resulting aluminum-rich layer was measured by four probes method after RIE treatment. Fig.4.13 shows the sheet resistance of the resulting aluminum-rich layers, Aluminum film of 200nm and ZnO:Al(AZO) coated glass annealed at 450^{o}C for 4h [8]. Recently, the formation of poly-Si seed layers on ZnO:Al coated glass using the ALILE process has introduced [9]. K. Y. Lee *et al.* studied the influence of the annealing temperature on the properties of the ZnO:Al they measured the electrical properties of bare ZnO:Al films on glass after annealing. The sheet resistance of annealed ZnO:Al film is significantly increased compare to aluminum-rich layers(Sample A,B and C). Also aluminum-rich layers as well as bare aluminum on glass show a low sheet resistance, as can be seen Fig. 4.13.

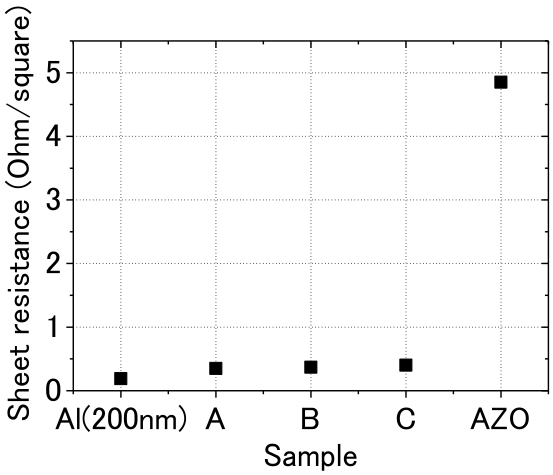

Fig.4.13 Sheet resistance of the resulting aluminum-rich layers, Aluminum film of 200nm and ZnO:Al(AZO) coated glass annealed at 450^{o}C for 4h [10].

Figure.4.14 (a) and (b) show the optical reflection and transmission spectra, respectively, for three different samples after removing the polycrystalline silicon layer on the top.

The reflectance is higher in the order of Sample C, B and A as shown in as show in Fig.4.14 (a). On the other hand, the transmittance is higher in the opposite order, Sample A, B and C as shown in Fig. 4.14 (b). The reflectivity spectra show pronounced dip around 850nm for all the samples, which arises from inter-band transitions in Aluminum. [11] This means the bottom layer was exchanged into aluminum after the crystallization. The transmission spectra for Sample A and B however were much higher than Sample C and an aluminum film, indicating the presence of aluminum depleted defects (holes) in the aluminum layer.

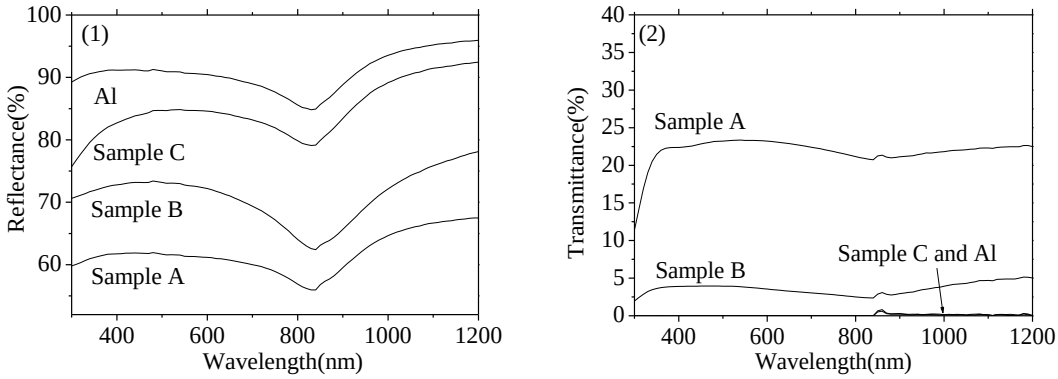

Fig.4.14 The optical (1) reflection and (2) transmission spectra, respectively, for Sample B, Sample C and Sample A after removing the polycrystalline silicon layer on the top.

4.5.4 Homogeneous in-plain distribution of Al

Figure.4.15 shows direct mapping of intensity of Al related signals in the EDX spectra obtained from Samples A, B and C in as-annealed states. The electron acceleration voltage was as low as 3.0keV for the selective detection of elements near the sample surface. These results indicate that Sample A shows most inhomogeneous in-plain distribution of Al, while Sample C is most homogeneous. The inhomogenerous contrast in Sample A is considered to arise from the presence of small Si crystallites within the newly evolved Al-rich layer as reported by Nast et al. for ALILE[12]. The origin of Si crystallites could be silicon that is not incorporated into the poly-Si layer. This is consistent with the optical reflection and transmission data in Fig.4.14.

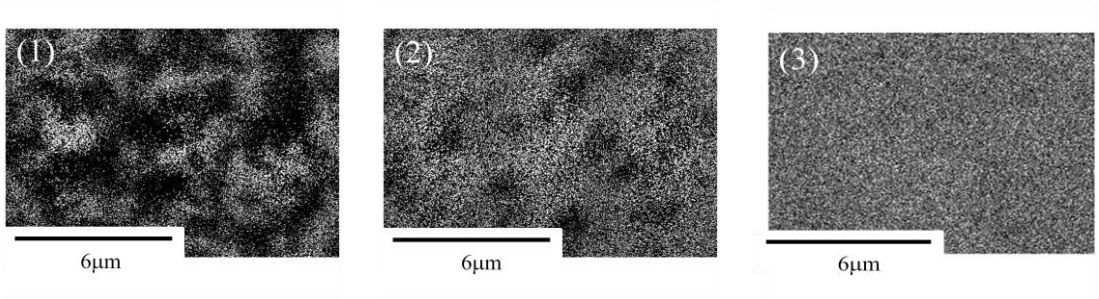

Fig.4.15 Direct mapping of intensity of Al related signals in the EDX spectra obtained from (1)Sample A,(2) B and (3) C in as-annealed states.

4.5.5 Influence on Al-rich layer by impurity

Depth profile of atomic concentration for oxygen and hydrogen in the film annealed at 450^{o}C for 24 hour was analyzed by SIMS as shown in Figs 4. Sample-(b) and -(c) (a-Si samples) were deposited on Sample B and Sample C (inverted-ALILE samples) under the identical conditions of sputtering for each sample, and therefore the results can be compared the impurity concentration between before and after crystallization. The impurity concentration of Sample A is showed by Kuraseko et al [13].

In XPS measurement, the content of oxygen is content at below 1 at.% in the balk region of poly layer. In Sample C, both of oxygen and hydrogen concentration show gradual increase in the deeper part of the sample. The origin of the impurity is considered to background impurity in the sputtering chamber, and the base pressure is decreased after deposition in sputtering. (1.2×10^{-2}Pa→2×10^{-3} Pa), which indicates the impurity concentration correspondingly decreasing toward the sample surface.

Since oxygen diffusion at annealing temperatures around 450^{o}C is very low, the depth profile of oxygen has a similar signature in amorphous silicon layer and Al-rich layer

that was originally amorphous silicon as shown in Fig.4.16. The peak in the oxygen content at around 400nm corresponds to the surface oxide after the crystallization. The oxygen content sharply decreases in the surface region for Sample B, while the content gradually decreases for Sample C. In the polycrystalline layer, the oxygen content is relatively lower and the second peak for oxygen is observed for both the Sample B and Sample C at around 600nm. Although the bottom part consists of multiple layers for Sample C, oxygen profile does not show any specific structure with keeping the original depth profile in amorphous silicon layer as mentioned above. On the other hand, the depth profile of hydrogen shows a simple structure, where hydrogen elimination mechanism during the crystallization.

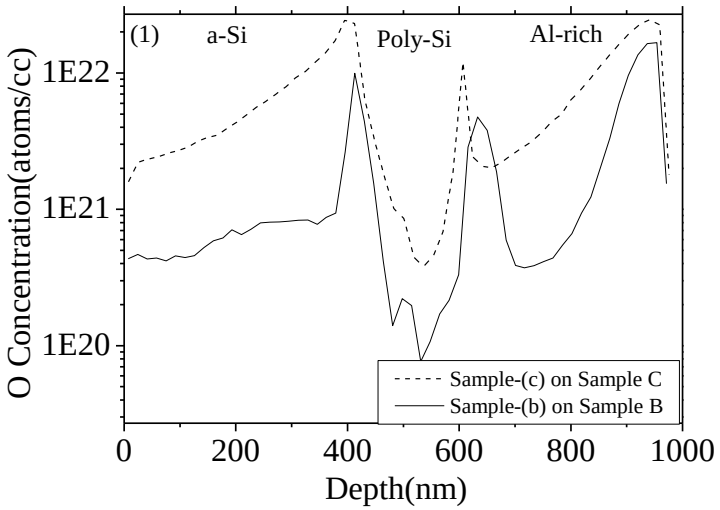

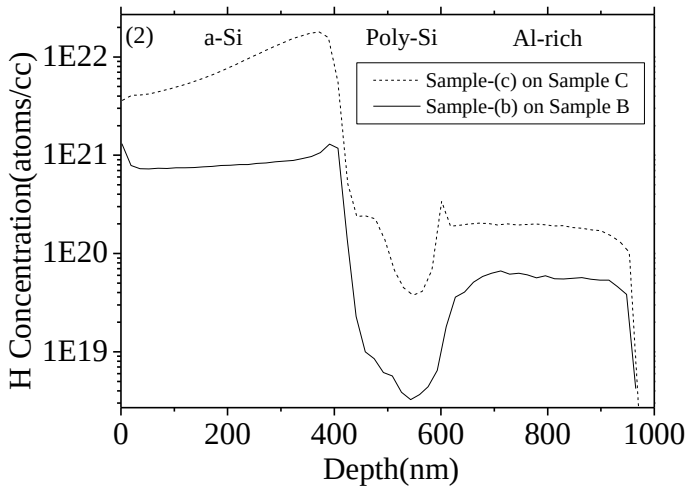

Fig.4.16 Depth profile of impurity concentration of sample used a-Si (Sample B and Sample C)/inverted-ALILE.

Figure 4.17 displays a cross-sectional bright-field TEM image for Sample C and cross-sectional mapping of Si and Al signal in the EDX spectrum. The EDX image shows the presence of four different layers in Fig.4.17-(2)-(3). The top layer is crystalline silicon layer on the alumina membrane layer formed by the layer exchange. The underlying layer, however, dose not consist of single aluminum layer as in conventional inverted-ALILE processes but of complex multi-layers of Al-rich/poly-Si/Al-rich with rather roughened interface. It is worth to point out uniform formation of Al-rich layer in Fig.4.17 without aluminum “hole” due to silicon precipitation.

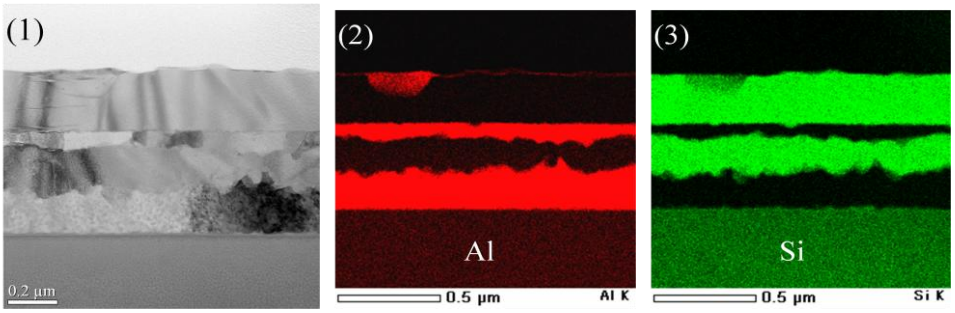

Fig.4.17 Cross-sectional bright-field (1)TEM image for Sample C and cross-sectional mapping of (2)Si and (3)Al signal in the EDX spectrum.

4.5.6 Growth times of the inverted-ALILE process

In this section, a model of the inverted-ALILE process is described. The nucleation and the subsequent growth can be observed directly during the layer exchange process, using an optical microscope equipped with a heating stage. Hence, the Al surface and the initial glass/a-Si interface can be studied through the transparent glass substrate. Due to the different reflectivity of Al and Si, it is possible to distinguish between these two materials (red and white areas correspond to poly-Si and Al, respectively). Also, it is possible to distinguish inside the initial glass/a-Si interface between these two materials (white and dark areas correspond to Al and a-Si, respectively).

Fig.4.18 shows the optical micrographs of the initial glass/a-Si interface and Al surface observed after various annealing times during an inverted-ALILE process at 450^{o}C. Figure.4.18(a1) shows the Al surface, 1min after the first dark spots were observed, with the optical microscope. The time when the first dark spots appear is referred to as nucleation time, which in this case amounts to 15min. Almost all grains, which correspond to the isolated red areas visible in Fig. 4.18 (a1) and Fig. 4.18 (c1), appeared

at the same time. With increasing annealing time, the size of Si grains increases, but there is only very little additional nucleation. This self-limitation of the nucleation is an important feature of the inverted-ALILE process. The Si grains grow uniformly in all lateral directions until they touch each other. Finally, a continuous poly-Si is formed (i.e., the whole optical micrograph appears red).

The crystallized fraction, which was defined as the ratio of the red area to total area in the optical micrographs, is shown in Fig. 4.19 as a function of the increasing annealing time for different between sample C (c1) and sample C (c2). The time difference is relatively larger than the time difference between sample A (a1) and sample A (a2). The grain growth of sample C was different nucleation time, which in this case amounts to 15min and 45min.

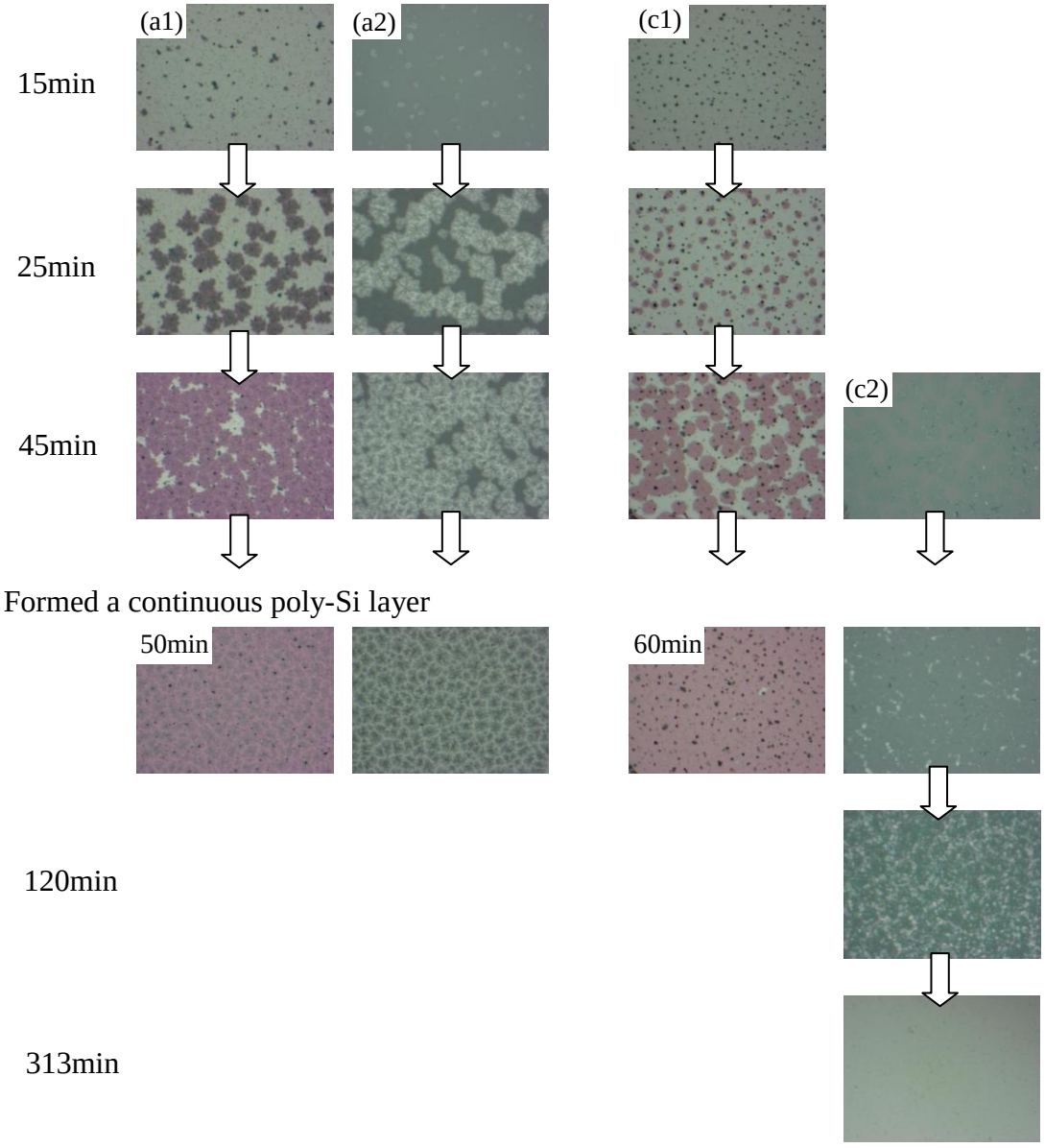

Fig.4.18 Inverted-ALILE by Sample C measured from the inside of Al layer and a-Si layer.

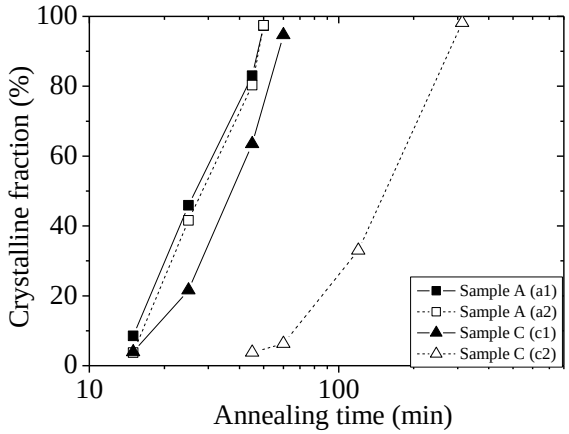

Fig 4.19 Evolution of crystalline fraction as a fraction of annealing time with various initial a-Si films observation from Al films and a-Si films side.

The crystallized fraction, which was defined as the ratio of the red area to total area in the optical micrographs, is shown in Fig. 4.19 as a function of the increasing annealing time for different between sample A and sample C . This result is similar to that of Ref.[14] related to ALILE process with a-Si:H and a-Si deposited by rf magnetron sputtering system. The influence of the precursor layer a-Si and a-Si:H on the properties of obtained films after the process of Al induced crystallization has been studies by Grigorov et al. [15].

The a-Si:H films crystalline at temperature lower than that of a-Si. Consequently, hydrogen acts as reducing the crystallization temperature. It was already reported that hydrogen facilities the crystallization of amorphous silicon, probably in interstitial positions [16]. It is supposed that protons stimulate the crystalline grain growth probably by increasing the diffusion rates of Al and Si, which exchange their places during ALILE [17]. Therefore, the a-Si:H films crystalline at times shorter than that of a-Si.

4.5.7 Model of the inverted-ALILE process

In order to demonstrate the diffuse of the Aluminum into a-Si for the layer exchange process, Sample A, Sample B and Sample C were prepared. To observe the diffusion of Al, the samples were annealed at 450^{o}C for 45min. After the annealing step, samples were cleaned by wet etching, which resulted in the elimination of initial aluminum layer and native oxidized aluminum layer at the sample surface. Acid solution is the mixed solution containing phosphoric acid, nitric acid, acetic acid and dilution water with the volume ratio of 16:1:2:1, respectively (standard solution for aluminum etching).

The samples were tilted by 45^{o} to show both cross section and surface. It shows that after inverted-ALILE processes, the sample surfaces were textured by irregularly-shaped micron-scale islands with various sizes. Since the samples were thoroughly etched by wet Al etching, these islands should not be Al particles. Sample A and Sample B show the isolated holes in underneath layer visible in Fig.4. 20. Sample C shows to prevent from forming the holes in the underneath layer.

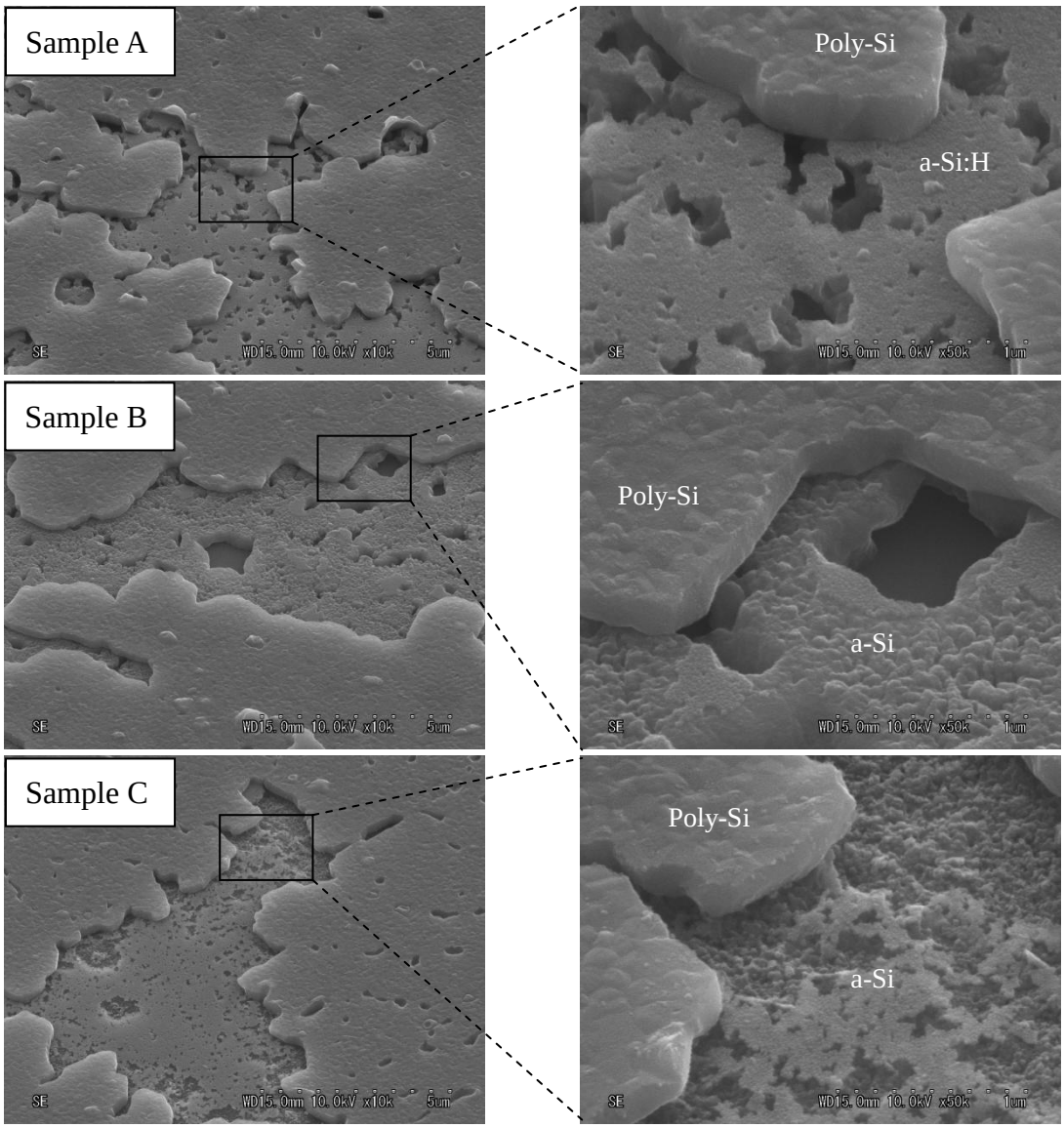

Fig.4.20 SEM images of Sample A, Sample B and Sample C were annealed for 45min at 45^{o}C. After the annealing step, the Al was etched off chemically.

The origin of the formation of complex structure is considered to be related with the presence of oxygen impurity in the amorphous silicon layer. The formation mechanism of Sample A, Sample B and Sample C shows in Fig. 4.21. First, the presence of the impurity disrupts crystallization of silicon in the amorphous layer and prevents from forming an optical “hole” in the Al-rich layer after the layer-exchange. Second, the

Al-rich layer grown underneath the AlOx membrane could form the oxide layer at a growth front due to oxygen in a-Si layer(Fig.4. 21 Sample C-(3)). The formation of oxide layer at the interface between the Al-rich and a-Si layers leads to the “secondary” layer exchange. The secondary exchange is speculated to occur successively after the primary layer exchange (Fig.4.21 Sample C-(4)). The observation of the temporal change of front surface suggests that the formation of silicon crystallites is completed in the first 45minuites, while the back side observation suggests that AL-rich layer seems to appear after the completion of the change in the front side. Thus the secondary layer exchange transforms the initial Al /AlOx /a-Si /glass substrate triple-layer into the poly-Si (1) /AlOx (1) /Al-rich (1) /poly-Si(2) /AlOx (2) /Al-rich (2) /glass substrate multi-layer. The thicknesses of the poly-Si (2) and Al-rich (2) layers are almost same, while the upper Al-rich (1) layer is thinner. The surface side interface between Al-rich and poly-Si is very flat because it was formed intentionally by the deposition of thin aluminum layer followed by natural oxidation, whereas the backside interface seems roughened due to the naturally formed interface during the layer exchange. In spite of the formation of multiple layers, the data shows the uniform formation of the Al-rich layer without any holes on the substrate for Sample C. Therefore the reflectance of Al-rich layer is about 80%. On the other hands, as shown in Fig.4.21-(1) columnar Al-rich layer with “gap” is formed in Sample A and thus reflectance of Al-rich layer is lowest (~60%).

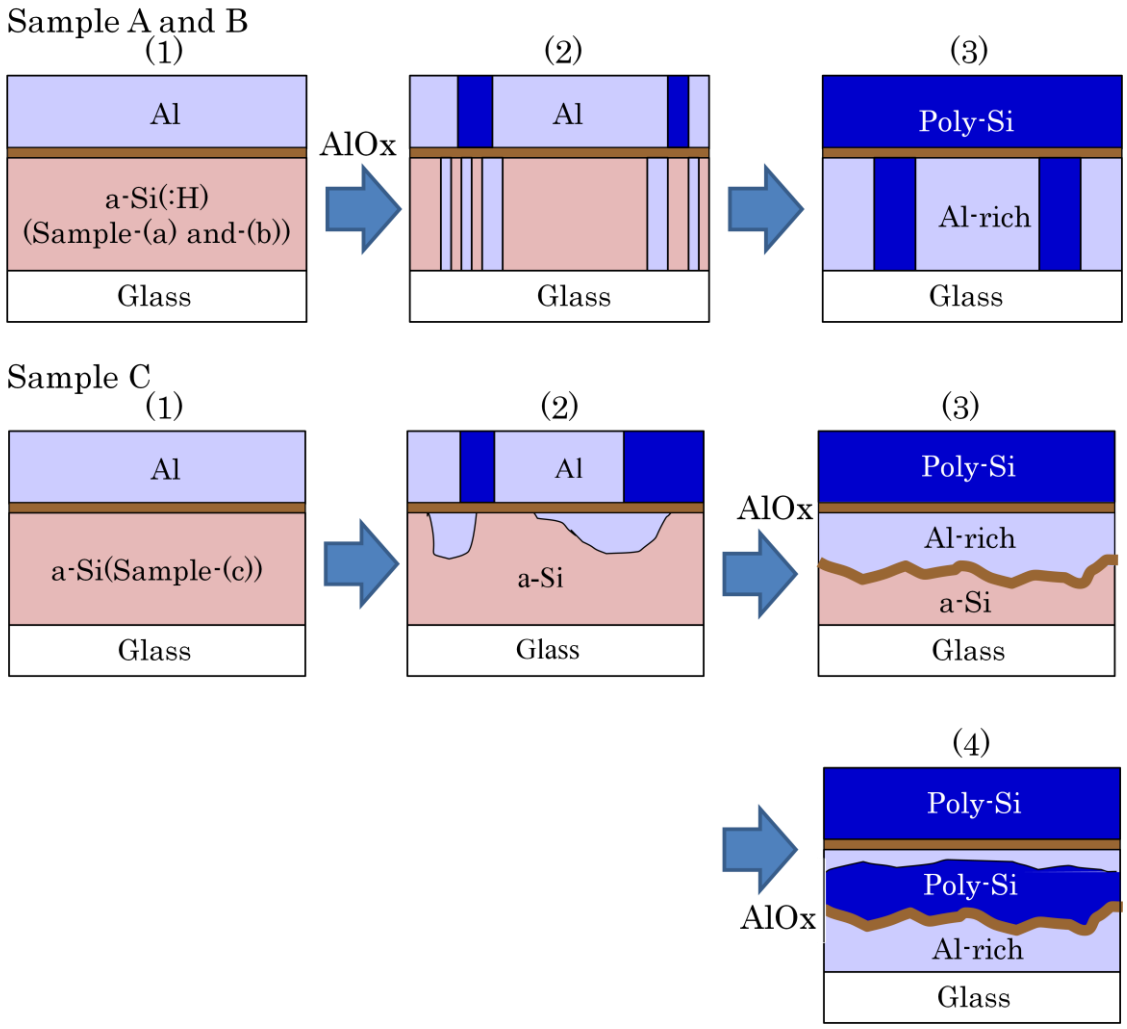

Fig.4.21 Model of the conventional inverted-ALILE (top) and the inverted-ALILE by a-Si including impurity (bottom)

4.6 Summary

This chapter has been investigated the uniformity of aluminum-rich layer in the inverted-ALILE process enhanced by the presence of impurity. The optical reflectance of Al-rich layer for the sample containing higher amount of oxygen impurity in a-Si was higher than that for the sample with less oxygen or for a-Si:H sample. SIMS

measurements and TEM observation for the most contaminated sample shows uniform formation of Al-rich layer in spite of the presence of multiple layers. The mechanism determining of the uniformity of Al-rich back reflector is discussed in terms of oxygen impurity and its relevance to the two step layer exchange process.

4.7 Reference

1. V. Grigorov, O. Angelov, M. Sendova-Vassileva, D. Dimova-Malinovska: Thin Solid Films, **511** (2006) 381.

2. H. Ehrenreich, H. R. Philipp, and B. Segall: Phys. Rev, **132** (1963) 1918.

3. O. Nast and S. R. Wenham: J. Appl. Phys, **716 (**2000) 724.

4. N. E. Lee, G. A. Tomasch, and J. E. Greene: Appl. Phys. Lett, **65** (1994) 3236.

5. B. Rau, I. Sieber, B. Selle, S. Brehme, U. Knipper, S. Gall, and W. Fuhs: Thin Solid Films, **451** (2004) 644.

6. J. Platem, B. Selle, I. Sieber, S. Brehme, U. Zeimer, and W. Fuhs: Thin Solid Films, **381**(2001) 22.

7. G. Ekanayake, T. Quinn, and H. S. Reehal: J. Cryst. Growth **293** (2006) 351

8. K. Y. Lee, M. Muske, I. Gordon, M. Berginski, J. D'Haen, J. Hupkes, S. Gall, B. Rech: Thin Solid Films, **516** (2008) 6869.

9. D. Dimova-Molinovsla, O. Angelov, M. Kamenova, A. Vaseashta, J. C. Pivin, J. Optoelectron: Adv. Matter, **9** (2007) 355.

10. K. Y. Lee, M. Muske, I. Gordon, M. Berginski, J. D'Haen, J. Hupkes, S. Gall, B. Rech: Thin Solid Films, **516** (2008) 6869.

11. H. Kuraseko, N. Orita, H. Koaizawa, M. Kondo: M. Appl. Phys. Express. **2** (2009)

015501.

12. F. Kezzoula, A. Hammouda, M. Kechouane, P. Simon, S.E.H. Abaidia, A. Keffous, R. Cherfi, H. Menari, A. Manseri, Applied Surface Science, 257, 9689, (2011).

13. V. Grigorov, O. Angelov, M. Sendova-Vassileva, D. Dimova-Malinovska: Thin Solid Films, **511** (2006) 381.

14. H. Shirai, J. Hanna, I. Shimizu: Jpn. Appl. Phys. **30** (1991) 679.

15. S. Sriraman, S. Agarwal, E.S. Aydil, D. Maroudas: Nature **62** (2002) 481.

16. P. I. Widenborg and A. G. Aberle: J. Cryst. Growth, **242** (2002) 270.

17. O. Nast, Ph.D. thesis, Philipps-Universität Marburg, 2000.

Chapter 5

Application of inverted-ALILE to thin film silicon solar cells

5.1 Introduction

In this section, inverted-ALILE sample applies to a thin film solar cell fabrication. Fabrication procedure and structure of a solar cell using inverted-ALILE sample is detailed. Solar cell performance is demonstrated and assumed challenges remaining in solar cell with inverted-ALILE sample for higher efficiencies are also shown.

5.2 Fabrication procedure of solar cell using inverted-ALILE

As show in Fig.5.1, thin film silicon solar cell having mesa structure was formed by using inverted-ALILE sample. Schematic procedure of solar cell fabrication with inverted-ALILE sample is explained as below.

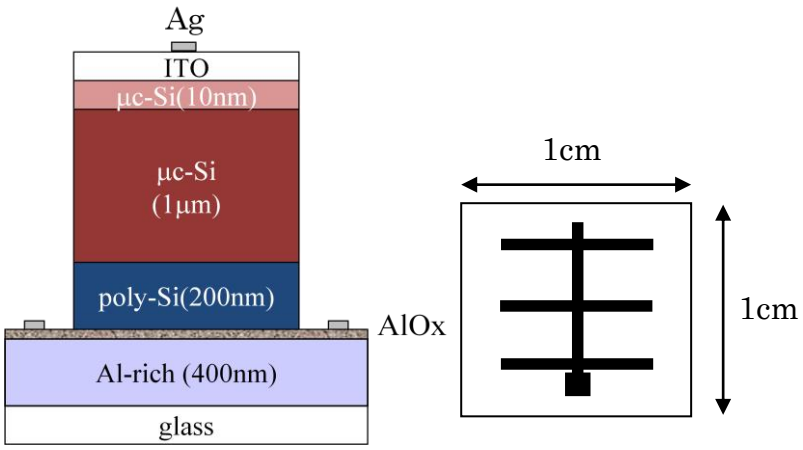

Fig. 5.1 Solar cell structure using inverted-ALILE sample

(1) Inverted-ALILE

A 400nm of a-Si layer was prepared on the glass substrate (Corning 1737). A 13nm of aluminum thin film was deposited on the sample surface, and exposed to ambient air for 1h in order to prepare the native oxidized aluminum interlayer. During air exposure, the sample was kept with room temperature (RT). Another aluminum layer was deposited on the sample. Thickness of another aluminum layer was 200nm. This precursor sample was annealed with the temperature of 450^{o}C and annealing time of 24 h in N_2 ambient. This sample is Sample C.

(b) Pre-cleaning (wet etching and H_2 plasma treatment)

As demonstrated in Fig.4.16, inverted-ALILE sample contains native oxidized aluminum layer on top of the sample surface. This oxidized aluminum layer results from native oxidization of surface of the aluminum layer before annealing and remains the

original position during the annealing. The phenomenon is similar to the interlayer of inverted-ALILE sample, which remains at the original position between the poly-Si and aluminum-rich layer during the annealing. This oxidized aluminum layer on top of the inverted-ALILE sample should be eliminated before i-layer deposition. Existence of native oxidized aluminum layer on top of the surface may cause decrease of solar cell performance due to larger series resistance of p-i-n structure solar cell. In this study, wet etching treatment with acid solutions was performed in order to eliminate native oxidized aluminum layer on top of sample surface. Solution consists of 2% hydrofluoric acid diluted with pure water. The sample was treated with hydrofluoric acid treatment was performed for 1min, and rinsed with pure water and dried with N_2 gas. The solution was used to eliminate the native oxidized silicon layer and the native oxidized aluminum layer of the sample surface. Hydrogen plasma treatment (H_2 flow rate: 380SCCm; RF power 25W; Time: 15min) was also performed before the following i-layer deposition in order to clean the surface of p-layer (Al doped poly-Si film).

(c) i-layer deposition

Multi-chamber type PECVD system was employed to prepare μc-Si:H i-layer, which acts as absorber layer of p-i-n structure solar cell. Source gas was mixed gas of SiH_4 and H_2, and the flow rate was 10.5 and 380SCCM, respectively. Structure temperature during deposition was kept at 180^{o}C and the working pressure was 1.5 Torr. RF(13.56MHz) power was 25W. Film thickness of i-layer was 1μm.

(d) n-layer deposition

N layer deposition was carried out after i-layer deposition. Source gas was a mixture gas of SiH_4, H_2 and PH_3. Flow rate was 3, 148 and 12 SCCM, respectively. Substrate temperature was 196^oC and working pressure was 0.3 Torr. A 60MHz of VHF power supply was employed for n-layer deposition. The output power was 50W. Film thickness of n-layer was 10nm.

(e)TCO deposition

In order to efficiently collect generated current with lateral direction, ITO was prepared on the surface of n-layer by sputtering. Thickness of ITO electrode was 80nm.

(f) Mesa etching

In order to reveal the bottom electrode (aluminum-rich metallic layer), RIE was performed, where ITO film was used as a soft mask. Source gas was a mixed gas of SF_6 and O_2. Flow rate was 100 and 20 SCCM, respectively. Working pressure was 20Pa and RF power was 200W. The treated time was 60s.

(g) A grid deposition

A 250nm of Ag grid electrode was prepared by DC sputtering on ITO electrode in order to compensate the poor electrical conductivity of ITO. The grid structure in this

study is shown in Fig. 5.1.

Solar cell structure fabricated with the process of (a)-(g) is also shown in Fig. 5.1. Area of solar cell was $1cm^2$(=1cm×1cm).

5.3 Performance of solar cell using inverted-ALILE

I-V characteristic and quantum efficiency of the fabricated solar cell are shown in Fig. 5.2. Jsc of 15.7mA/cm2, Voc of 0.412V, FF of 0.693 and conversion efficiency of 4.5 % were demonstrated under illumination of calibrated light source (AM 1.5, $100mW/cm^2$, RT) without any optical confinement techniques. Especially, Jsc of 15.2 mA/cm^2 seem to be lower than that obtained by solar cells with inhomogeneous back reflector, which have shown 15.7 mA/cm^2. Two possible reasons are considered for the lower performance of solar cell with inverted-ALILE in short circuit current. One is that the poly-Si layer with contamination increases carrier recombination. Inverted-ALILE sample contains an aluminum-rich bottom electrode between glass substrate and the obtained poly-Si layer. Therefore, the solar cell fabricated with inverted-ALILE sample can be formed into sandwich structure. In the case of sandwich structure, a p-i-n layer stack is located between two electrodes in a straight line so that carriers generated by incident light run along grain boundaries. As a result, recombination rate of carrier can be suppressed and generated carrier can be efficiently collected to electrodes. Sample C has impurity in poly-Si layer as a shown in Fig.4.16 so that much recombination in poly-Si seed layer and result in lower open circuit voltage and conversion efficiency. The other possible reason is that a Al reflecting layer is between glass substrate and the

poly-Si layer. Solar cell with Sample A can not be fabricated a high reflectance layer, so that an amount of incident light is transmitted through the absorber layer in the solar cell. In contrast, solar cell with Sample C has a high reflectance layer between glass substrate and the poly-Si layer. As shown in Fig. 4.14, the reflecting layer fabricated by inverted-ALILE process indicates a high reflectance in the visible light region. Therefore, the existence of the reflecting layer leads to an increase of light absorption and short circuit current. Due to these two reasons, larger short circuit current is realized by using inverted-ALILE than by using conventional ALILE[1].

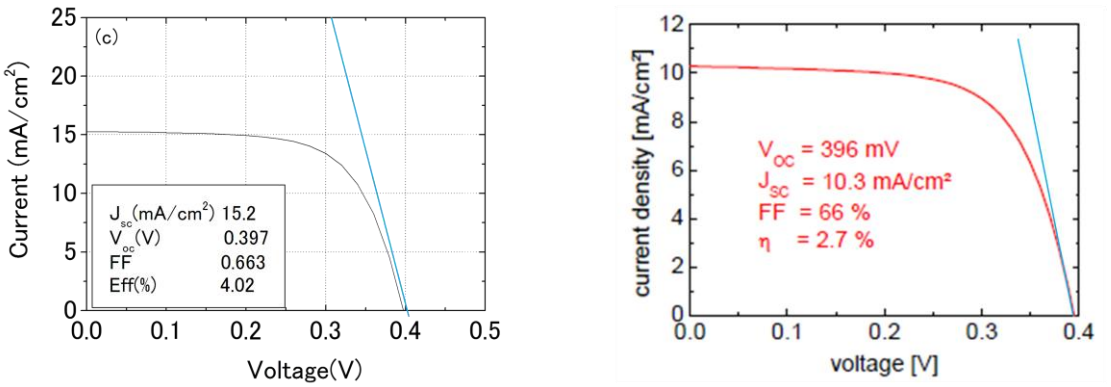

Fig.5.2 I-V and QE characteristic of solar cell with inverted-ALILE (left) vs ALILE(right).

Table.5.1 I-V characteristic data of solar cell with inverted-ALILE vs ALILE.

	Sample C	ALILE cell*
Jsc (mA/cm2)	15.2	10.3
Voc (V)	0.397	0.396
FF	0.663	0.66
η (%)	4.02	2.7
Series resistance (Ω·cm²)	4×10^{-3}	6.25×10^{-3}

5.4 Challenges approaching in inverted-metal induced crystallization solar cells for higher efficiency

5.4.1 Epitaxial breakdown of the absorber layer

It was confirmed that the sample obtained by inverted-ALILE process has a poly-Si layer with large grain size and a preferential (100) orientation, which is advantageous to following low temperature epitaxial growth of silicon film. Solar cell efficiency with epitaxial breakdown of i-layer will be quite lower as compared with that with epitaxial growth i-layer owing to higher crystallinity and larger grain size. Therefore, it is necessary for high efficiency thin film silicon solar cells with inverted-ALILE to effectively employ inverted-ALILE sample as seed layer and realize low temperature epitaxial growth of the absorber layer.

5.4.2 Silver-induced layer exchange

The eutectic temperature of the Si/Al alloy system (836^{o}C) is significantly higher than of the Si/Al system (577^{o}C) [2]. The equilibrium solubility of silver in silicon is reported to be negligibly small [3] , and therefore, metal-induced crystallization with silver should lead to intrinsic films. Scholz et al. show similar to the Al/Si system, also in the Ag/Si system a layer exchange process has been achieved. The sample was annealed at 530^{o}C for 3hours. The appearance of their report for the polycrystalline films indicated a good crystalline and electronic quality of the film.

A reflectance of silver film has higher than that of aluminum [4]. A resistivity of silver

film has lower than that of aluminum. A precursor structure with a layer stack of glass/a-Si/Ag is employed for inverted-Ag induced layer exchange (inverted-AgILE). Invered-AgILE process is expected to form the final layer structure of glass/Ag-rich/poly-Si from the precursor sample structure of glass/a-Si/Ag. After annealing, poly-Si layer is formed on the top surface of the sample and an silver-rich metallic layer with a small portion of silicon is fabricated between the poly-Si layer and the glass substrate. As a result, the obtained solar cell has a highly conductive metallic layer at the bottom, which can act as a bottom electrode for solar cells. The existence of silver-rich layer on insulating substrate allows a sandwich structure solar cell, which is more favorable for high efficiency solar cell than the aluminum-rich layer obtained by the inverted-ALILE process. Moreover, silver-rich metallic layer existing between the insulating substrate and the poly-Si layer can be used as a reflecting layer, so that effective light trapping and higher current density is expected.

Due to the highly p-type polycrystalline silicon ($p \geq 10^{18} cm^{-3}$) [5], whereas AgILE result in intrinsic polycrystalline silicon. The initial doping of the a-Si with boron and phosphorus is necessary. Antesberger et al show the boron-doped poly-Si layer of conventional AgILE is obtained. The mobility of the poly-Si is at $p=4\times10^{18} cm^{-3}$. From these results, boron-doped poly-Si is expected for formed glass substrate with silver-rich film. If inverted-AgILE with boron-doped poly-Si sample is applied to thin film silicon solar cell fabrication, the solar cell indicate the potential of inverted-AgILE for high efficiency thin silicon solar cells.

5.5 Summary

In this chapter, inverted-ALILE sample was applied to p-i-n type thin film silicon solar cell fabrication with Al-rich layer of high reflectance. Procedure of solar cell fabrication and solar cell structure using inverted-ALILE sample were explained. It was demonstrated that the poly-Si layer of inverted-ALILE sample can effectively acts as p-layer for p-i-n solar cells and the aluminum-rich layer between the poly-Si layer and glass substrate can function as a bottom electrode and a reflecting layer. It was also show that higher short circuit current was obtained compared with that of conventional ALILE. It was confirmed that inverted-ALILE has a possibility for high efficiency thin films silicon solar cells.

5.6 Reference

1. S. Gall, K.Y. Lee, P. Dogan, B. Gorka, C. Becker, F. Fenske, B. Rau, E. Conrad, B. Rech, 22nd European Photovoltaic Solar Energy Conference, 3-7 September 2007, Milan, Italy

2. J. L. Murray and A. L. McAlister, Binary Alloy Phase Diagrams (American Society of Metals, Metals Park, OH, 1986).

3. F. Rollert, N. A. Stolwijk, and H. Mehrer, J. Appl. Phys. D 20 1148 (1987).

4. A. Mc Leod .Thin film optical filters, A. Hilger, London, (1985).

5. T. Antesberger, T. A. Wassener, M. Kashani, M. Scholz, R. Lechner, S. Matich, and M. Stutzmann, J. Appl. Phys. 112, 123509 (2012).

Chapter 6

Conclusions

A crystallization method of amorphous silicon, an inverted aluminum-induced layer exchange (inverted-ALILE) method, had been studied in order to achieve high efficiency thin-film poly-Si solar cells on insulating substrates. By using inverted-ALILE process, large grained and high crystallinity poly-Si thin film can be obtained on insulating substrates, especially on low-cost glass substrates.

The crystal orientations of grown poly-Si on Al layers were controlled to (111) or (100) by modulating the Al/Si thickness. The surface of the obtained poly-Si indicates (100) preferential orientation, which is favorable to following low-temperature epitaxial growth of silicon. We had found that the ratio of preferential orientation depends on the thickness of precursor Al. The precursor inverted-ALILE sample in initial annealing, γ-Al_2O_3(111) is formed at the surface of precursor Al layer. Crystalline silicon is known to form preferentially (111) face, Si(111) crystals tends to grow on γ-Al_2O_3(111) membrane. In case of precursor Al layer is thick, Si crystal is difficult to grow on the γ-Al_2O_3(111) membrane. In contrast, Si(100) crystals tend to grow on amorphous-Al_2O_3 membrane. Therefore, the Si crystal orientation is dominated by AlOx membrane. These results were explained on the basis of model considering the phase transition of the interfacial Al oxide layers. This process provided the orientation-controlled Si templates on insulating substrates, which enables successive Si crystal growth with high (100) orientation for epitaxial growth at low temperature.

In this thesis, precursor a-Si of inverted-ALILE process was discussed. It was found

that uniformity of aluminum-rich layer in the inverted-ALILE process was enhanced by the presence of impurity in precursor a-Si. SIMS measurements and TEM observation for the most high impurity concentration sample showed uniform formation of aluminum-rich layer in spite of the presence of multiple layers. The mechanism determining of the uniformity of aluminum-rich layer is discussed in terms of oxygen impurity and its relevance to the two step layer exchange process. Therefore, the optical reflectance of aluminum-rich layer for the sample containing higher amount of oxygen impurity in a-Si was higher than that for the sample with less oxygen or for a-Si:H sample. Additionally, p-i-n structure solar cells were fabricated with inverted-ALILE samples (Sample C). The solar cell of inverted-ALILE was fabricated with the high optical reflectance of Al back reflector. From the result of I-V characteristic, higher short circuit current was demonstrated than that of solar cells with conventional ALILE. It was suggested that inverted-ALILE possesses an attractive possibility to realize high efficiency thin film silicon solar cells.

Research reports

List of publications

1. “Impurity driven multilayer formation in inverted aluminum-induced layer exchange of silicon”, Masayoshi Takeuchi, Michio Kondo: Japanese Journal of Applied Physics, accepted.

List of publication (co-author)

1. C. Jaeger, T. Matsui, M. Takeuchi, M. Karasawa, M. Kondo, M. Stutzmann “Thin Film Solar Cells Prepared on Low Thermal Budget Polycrystalline Silicon Seed Layers” Japanese Journal of Applied Physics, (2010)

List of Presentations

1. Masayoshi Takeuchi, Michio Kondo “Study on Inverted-Aluminum induced Layer Exchange process for Thin film poly-Si Solar Cells”, The Japan Society of Applied Physics and Related Societies, The 70th Fall Meeting (2009)

2. Masayoshi Takeuchi, Michio Kondo “Study on Inverted-Aluminum induced Layer Exchange process for Thin film poly-Si Solar Cells”, The Japan Society of Applied Physics and Related Societies, The 71th Fall Meeting (2010)

3. Masayoshi Takeuchi, Takehiko Nagai, Hitoshi Sai, Ivan Turkevych, Michio Kondo "Inverted-ALILE Process for Thin Film Si Solar Cells", 24th International Conference on Amorphous and Nanocrystalline Semiconductors (2011)

4. Masayoshi Takeuchi, Michio Kondo "Study on Inverted-Aluminum induced Layer Exchange process for Thin film poly-Si Solar Cells", The Japan Society of Applied Physics and Related Societies, The 72th Fall Meeting (2012)

Acknowledgements

This work was performed at Advanced Low Cost Processing Team (ALOCOP), Research Center for Photovoltaic Technology (RCPVT) of National Institute of Advanced Industrial Science and technology (AIST) under the supervision of Professor Michio Kondo.

I would like to express my deepest appreciation and gratitude to my supervisor, Professor Michio Kondo, for giving a change for this study, providing valuable guidance, instruction, beneficial suggestions and useful advice as well as continuous support and encouragement throughout this work.

I am extremely grateful to Professor Osamu Odawara and Professor Hiroyuki Wada in Tokyo Institute of Technology for providing valuable suggestions, kind advices and supports.

I am grateful to Professor Mamoru Yoshimoto and Professor Jun-ichi Hanna in Tokyo Institute of Technology for providing valuable suggestions, kind advices and supports.

I would like to give my gratitude to Dr. Takehiko Nagai, Dr. Takashi Koida, Dr Takuya Matsui, Dr Hitoshi Sai, Dr Hidenori Mizuno, Dr Shota Nunomura, Dr Kimihiko Saito (Hukushima University), Dr. Noge hiroshi (Hukushima University), Dr Testuya Kaneko (Hukushima University), Dr. Tetsuhiko Miyadera, Dr. Yosei Sibata of the Natial Institute of Advanced Industrial Science and technology (AIST) for their valuable suggestions and kind advices throughout this work.

I benefited significantly from suggestions made by Professor Masao Isomura (Tokai University), Dr. Junko Habasaki (Tokyo Institute of Technology) and Dr. Hanna Hubarevich (Tokyo Institute of Technology).

I am further grateful to Ms. Yoshiko Miyanuma, Ms. Emi Tsuji and Ms. Emiko Izumi and Ms. Junko Tsukamoto for their kind and useful support throughout this work.

I am grateful to my colleagues in the Michio Kondo and Yuji Yoshida laboratory, the Osamu Odawara laboratory, the Hiroyuki Wada laboratory and the Michio Kondo laboratory, Mr. Yoshirnori Aoyama, Mr. Daiki Tanaka, Mr. Takashi Nunokawa, Ms. Pattarin Chewchinda, Mr. Kunio Fujii, Mr. Takamaro Malik Matsuda, Mr. Shou Koyama, Mr. Junpei Iwasaki, Mr. Rigaku Hiraoka, Mr. Tomohiro Ikehata, Mr. Kousuke Kawazoe, Mr. Nobutaka Tanishima, Mr. Tatsuya Numa, Mr. Kazuhei Hayashi, Mr. Kazuki Mori, Mr. Satoshi Yone and Mr. Kazuhiro Gotoh.

I am especially grateful to Mr. Kenkichi Matsuno (AIST), Mr. Hirobumi Morita (Oxford Instruments Co., Ltd), Mr. Gento Misawa (AIST) and Dr. Hiroyuki Akinaga (AIST) for their advices, support and encouragement throughout this work.

I would like to express my deep gratitude to The Research Center for Photovoltaic Technology and The Nano-Electronics Research Institute of AIST for generous support.

Finally, I would like to thank my father, sister, brother and mother for continuous and warm support and encouragements throughout this work.